

Matrix function-based centrality measures for layer-coupled multiplex networks

KAI BERGERMANN* AND MARTIN STOLL

*Chair of Scientific Computing, Department of Mathematics, Technische Universität Chemnitz,
09107 Chemnitz, Germany*

*Corresponding author: kai.bergemann@math.tu-chemnitz.de

[Received on 30 April 2021]

Centrality measures identify the most important nodes in a complex network. In recent years, multilayer networks have emerged as a flexible tool to create increasingly realistic models of complex systems. In this paper, we generalize matrix function-based centrality and communicability measures to the case of layer-coupled multiplex networks. We use the supra-adjacency matrix as the network representation, which has already been used to generalize eigenvector centrality to temporal and multiplex networks. With this representation, the definition of single-layer matrix function-based centrality measures in terms of walks on the networks carries over naturally to the multilayer case. Several aggregation techniques allow the ranking of nodes, layers, as well as node-layer pairs in terms of their importance in the network. We present efficient and scalable numerical methods based on Krylov subspace techniques and Gauss quadrature rules, which provide a high accuracy in only a few iterations and which scale linearly in the network size under the assumption of sparsity in the supra-adjacency matrix. Finally, we present extensive numerical studies for both directed and undirected as well as weighted and unweighted multiplex networks. While we focus on social and transportation applications the networks' size ranges between 89 and $2.28 \cdot 10^6$ nodes and between 3 and 37 layers.

Keywords: Centrality measures, communicability measures, multiplex networks, matrix functions, Krylov subspace methods, Gauss quadrature

2000 Math Subject Classification: 05C50, 05C82, 15A16, 65F60, 91D30, 94C15

1. Introduction

The study of complex networks has been a thriving interdisciplinary field of research for many decades where some of the most impactful results found their way into our daily life [7, 16, 41, 45, 55]. Applications of network science range from biology, chemistry, and physics over engineering and economics to the social sciences [20, 37]. In recent years, much effort has been devoted to the generalization of established graph-based methods to the case of multilayered structures, cf. e.g. [13, 14, 37, 43, 51–53]. These allow entities to interact in several different ways or reflect changing relationships over time leading to ever more realistic models of highly complex phenomena.

Besides the study of community structure and the modeling of dynamical processes on complex networks the detection of the most central nodes, i.e. entities, has been a topic of great importance in network science. A variety of centrality measures has been proposed over recent decades including degree centrality, betweenness centrality [25], closeness centrality [26], and eigenvector centrality [15]. Successful variants of eigenvector centrality were developed in the context of the early internet [16, 38, 45].

This paper addresses the class of matrix function-based centrality measures, which has been studied

intensively for single-layered networks, cf. [9, 19, 22, 23, 36] as well as the recent review article [8]. These parameterized measures can be tuned to emphasize subgraphs of different sizes and have been shown to include the (local) degree and the (global) eigenvector centrality measures as limit cases [12]. In practice, different matrix function-based centrality measures often yield similar but not equal node rankings. However, parameter-dependent relations between different measures could be shown in [2]. A very closely related set of matrix function-based quantities is given by communicability measures [11, 21, 22]. We equally include these in our discussion due to their similarity both mathematically as well as in terms of their interpretation in the network application. We allow both directed and undirected edges in all networks and differentiate between each entity's role as broadcaster and receiver in the case of directed networks.

The main contribution of this paper is the generalization of matrix function-based centrality and communicability measures to a special class of multilayer networks. The major difference to single-layer networks is that these not only contain intra-layer edges between nodes from the same layer but also inter-layer edges between nodes belonging to different layers. While it is not required from a theoretical perspective we restrict ourselves to layer-coupled multiplex networks in which inter-layer edges are only allowed between instances of the same physical node, i.e. copies of the same node in different layers, and where the edge weight between any pair of layers is fixed for all inter-layer edges between them. This choice of multilayer network structure is particularly well-suited to create meaningful multilayer networks from multiple single-layer networks on the same set of nodes where no notion of inter-layer edges is present in the data.

In the context of non-backtracking walks [1] a relation of matrix function-based centrality measures to certain three-layer networks has been discovered in [4, 5]. However, this paper is to the best of our knowledge the first to apply matrix function-based centrality measures to a general class of multilayer networks. The formal representation of multilayer networks is a non-trivial task [37] and for this paper we choose the representation in terms of a supra-adjacency matrix. The same representation has already been successfully used to generalize eigenvector centralities to the case of temporal and multiplex networks [51–53]. Other approaches for generalizing eigenvector centrality to the multilayer case include using the network's representation in terms of an adjacency tensor and computing its largest eigentensor [54, 56]. The development of tensor function-based centrality measures for the tensor representation of multilayer networks is an interesting road for future research.

The multiplex framework considered in this work supports the representation of temporal networks where the layers represent a certain relationship between the nodes at different points in time. For this type of network, our approach provides the averaged importance of nodes over the given time period. For certain applications in which the temporal development of a relationship should be accounted for, dynamical network approaches may be a more favorable choice [6, 8, 18, 33].

As we use a linear algebraic formulation of the considered multilayer graphs in terms of their supra-adjacency matrices, well-studied methods from numerical linear algebra can be put to new use as it is currently the case in many data-driven applications [49]. In particular, Krylov subspace methods for the approximation of matrix functions provide very mature computational means to evaluate matrix function-based centrality measures even for large-scale problems [31, 35, 47]. It will be shown that under the assumption of sparsity in the supra-adjacency matrix, which is usually not very restrictive in the context of complex networks, the runtime of all presented centrality measures scales linearly in the network size. A particularly elegant technique, which can be applied to compute lower and upper bounds on certain matrix function-based centralities, is given by the connection between Gauss quadrature, the Lanczos method, and orthogonal polynomials discussed by Golub and Meurant in [27–29, 32]. This has been applied to more classical numerical linear algebra problems, cf. e.g. [10, 30]. Many of the

presented computational methods have already been successfully applied to the evaluation of matrix function-based centrality measures on single-layer graphs [8].

The remainder of this paper is organized as follows. In Section 2 we introduce our multilayer framework including its representation in terms of the supra-adjacency matrix. Section 3 introduces existing matrix function-based centrality measures in the context of single-layer graphs. In Section 4 we generalize these centrality measures to the case of layer-coupled multiplex networks and establish aggregation concepts required for the interpretation of the obtained measures in the multilayer case. Section 5 then presents efficient numerical methods for the approximation of all introduced centrality measures for both directed and undirected as well as weighted and unweighted networks. Finally, Section 6 presents extensive numerical experiments on different real-world data sets covering a large spectrum of networks of different types and sizes. We analyze social, communication, as well as transportation networks with the number of nodes ranging from 89 to $2.28 \cdot 10^6$ and the number of layers from 3 to 37. While relatively small directed and undirected data sets allow the explicit computation of the involved matrix functions and consequently an error analysis of our proposed numerical methods, we also discuss specific issues of large-scale network computations, some of which can still be conducted on an average laptop with runtimes of only several seconds.

2. Multilayer graph representation

We start by introducing multilayer networks as well as their matrix representation in the form of supra-adjacency matrices. In terms of the general framework of multilayer networks introduced in [37], we restrict ourselves to node-aligned multiplex networks with one aspect (sometimes called “dimension”) and diagonal inter-layer coupling (cf. Figure 1b for an exemplary illustration). Both intra-layer and inter-layer edges are allowed to be either directed or undirected as well as weighted or unweighted, but we restrict ourselves to unsigned graphs, i.e. positive edge weights. In the following we elaborate on these concepts in more detail and introduce the notation. Note that we use the terms “graph” and “network” as well as “nodes” and “vertices” synonymously.

Multilayer graphs can be viewed as a set of single-layer graphs where edges can be present between nodes belonging to the same layer and between nodes belonging to different layers. Typically, the different layers represent different kinds of interactions between its entities. We first focus on *intra-layer edges*, i.e. edges between nodes within the same layer. We denote the number of graph layers by L and describe each single layer with the usual graph notation $\mathcal{G}^{(l)} = (\mathcal{V}^{(l)}, \mathcal{E}^{(l)})$, $l = 1, \dots, L$ with $\mathcal{V}^{(l)}$ denoting the *vertex set* of graph layer l and $\mathcal{E}^{(l)} \subset \mathcal{V}^{(l)} \times \mathcal{V}^{(l)}$ the *edge set* containing the connections between pairs of vertices $(x_i^{(l)}, x_j^{(l)})$ belonging to $\mathcal{V}^{(l)}$. We call x_i a *physical node*, which is represented by different instances $x_i^{(l)} \in \mathcal{V}^{(l)}$ of itself called *node-layer pairs* in the different layers $l = 1, \dots, L$. We assume all multiplex networks to be node-aligned, i.e. $\mathcal{V}^{(l)} = \mathcal{V}^{(k)}$ for all $l, k \in \{1, \dots, L\}$ so that each layer contains each physical node exactly once. If this property is not fulfilled for a given multilayer graph, we consider the union of vertices $\tilde{\mathcal{V}} = \bigcup_{l=1}^L \mathcal{V}^{(l)}$, define the number of nodes per layer as $n = |\tilde{\mathcal{V}}|$, and enforce $\tilde{\mathcal{V}} = \mathcal{V}^{(1)} = \dots = \mathcal{V}^{(L)}$ by adding isolated node-layer pairs $x_i^{(l)} \in \mathcal{V}^{(l)}$ with $(x_i^{(l)}, x_j^{(l)}) \notin \mathcal{E}^{(l)}$ for all $j = 1, \dots, n$ where necessary. Unless stated otherwise, we exclude self-edges in the intra-layers by requiring $(x_i^{(l)}, x_i^{(l)}) \notin \mathcal{E}^{(l)}$ for all $x_i^{(l)} \in \mathcal{V}^{(l)}$.

In this paper, edges can both be weighted or unweighted. For both cases, we introduce weight functions $w^{(l)} : \mathcal{V}^{(l)} \times \mathcal{V}^{(l)} \rightarrow \mathbb{R}_{\geq 0}$, not necessarily equal for all $l = 1, \dots, L$. In the unweighted case,

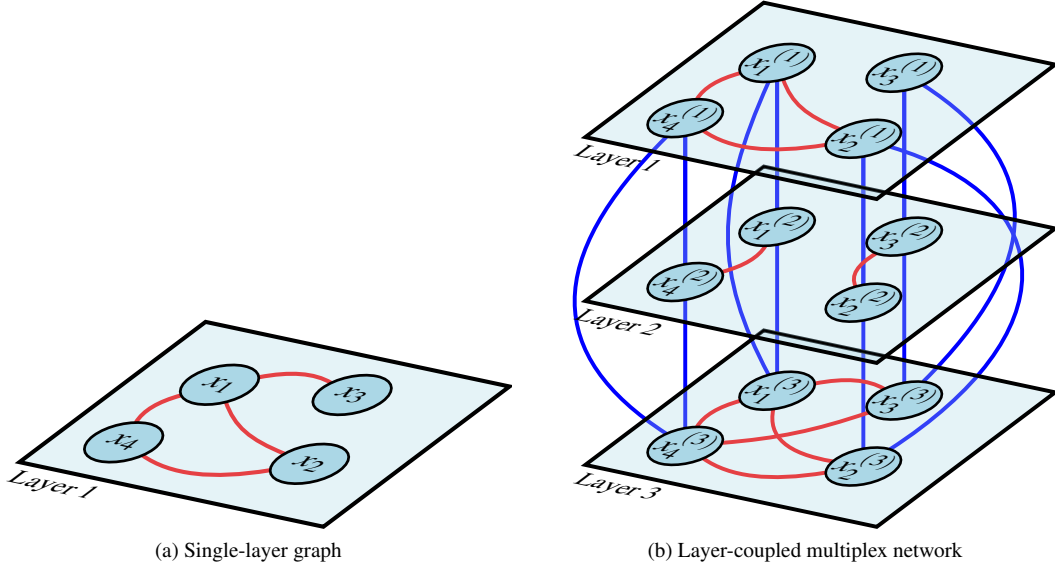


FIG. 1. Left: Example of a single-layer graph with 4 nodes. Right: Example of a layer-coupled multiplex network with 4 nodes and 3 layers. Intra-layer edges are marked red and inter-layer edges are marked blue.

we define

$$w^{(l)}(x_i^{(l)}, x_j^{(l)}) = \begin{cases} 1 & \text{if } (x_i^{(l)}, x_j^{(l)}) \in \mathcal{E}^{(l)}, \\ 0 & \text{otherwise.} \end{cases}$$

In the weighted case, we extend the definition to allow $w^{(l)}(x_i^{(l)}, x_j^{(l)}) \in \mathbb{R}_{>0}$ if $(x_i^{(l)}, x_j^{(l)}) \in \mathcal{E}^{(l)}$. In either case, we define the *single-layer adjacency matrices* $\mathbf{A}^{(l)} \in \mathbb{R}^{n \times n}$ for $l = 1, \dots, L$ via

$$\mathbf{A}_{ij}^{(l)} = w^{(l)}(x_i^{(l)}, x_j^{(l)}). \quad (2.1)$$

Furthermore, we will consider both directed and undirected graphs. Undirected edges depict a symmetric relation between the vertices so that we have $w^{(l)}(x_i^{(l)}, x_j^{(l)}) = w^{(l)}(x_j^{(l)}, x_i^{(l)})$ for all intra-layer edges. This property does not hold for directed networks where an edge can point from $x_i^{(l)}$ to $x_j^{(l)}$ but not from $x_j^{(l)}$ to $x_i^{(l)}$ or where edges can be present in both directions but carry different weights. Note that this leads to $\mathbf{A}^{(l)} = (\mathbf{A}^{(l)})^T$ for all $l = 1, \dots, L$ for undirected networks, which is not true for directed networks.

In addition to the intra-layer edges encoded in Equation (2.1), multilayer graphs may also contain *inter-layer edges*, i.e. edges between nodes belonging to different layers. This requires the definition of the *inter-layer edge set* $\tilde{\mathcal{E}} \subset \mathcal{V}^{(l)} \times \mathcal{V}^{(k)}$ containing inter-layer edges $(x_i^{(l)}, x_j^{(k)})$ where $l \neq k$. While theoretically all methods presented in this paper should also be applicable to general inter-layer edges, we restrict ourselves to diagonal layer coupling. This means that each node is only allowed to form an inter-layer edge to instances of itself in other layers and not to different physical nodes in other layers. Formally, this means that we only allow inter-layer edges $(x_i^{(l)}, x_j^{(k)})$ where $l \neq k$ and $i = j$.

This construction allows the creation of meaningful multilayer network representations for data sets without an inherent notion of inter-layer edges. The different layers could, for instance, represent social interactions between the same set of individuals on different platforms where interactions between any two individuals across platforms are impossible but the fact should be represented that each individual can move across platforms by the means of inter-layer edges.

This now gives us all the ingredients to define our (node-aligned) *layer-coupled multiplex network* consisting of a vertex set as well as intra- and inter-layer edge sets as $\mathcal{G} = (\mathcal{V}, \mathcal{E}^{(1)}, \dots, \mathcal{E}^{(L)}, \tilde{\mathcal{E}})$. There is a multitude of different multilayer graph representations available in the literature, cf. [37] for an overview. For this paper, we choose a supra-adjacency representation [37, Section 2.3]. Note that our construction corresponds to the special case of the supracentrality matrix defined in [53, Definition 3.1] where the centrality matrices are given by the single-layer adjacency matrices.

We start describing the supra-adjacency representation by collecting all intra-layer adjacency matrices $\mathbf{A}^{(1)}, \dots, \mathbf{A}^{(L)}$ defined in Equation (2.1) in a block-diagonal *multilayer intra-layer matrix* $\mathbf{A}_{\text{intra}} \in \mathbb{R}^{nL \times nL}$ which is defined by

$$\mathbf{A}_{\text{intra}} = \text{blkdiag}[\mathbf{A}^{(1)}, \dots, \mathbf{A}^{(L)}] = \begin{bmatrix} \mathbf{A}^{(1)} & \mathbf{0} & \dots & \mathbf{0} \\ \mathbf{0} & \mathbf{A}^{(2)} & \dots & \mathbf{0} \\ \vdots & \vdots & \ddots & \vdots \\ \mathbf{0} & \mathbf{0} & \dots & \mathbf{A}^{(L)} \end{bmatrix},$$

with $\mathbf{0} \in \mathbb{R}^{n \times n}$ the zero matrix.

Additionally, we define an inter-layer adjacency matrix. As by our previous discussion we require $(x_i^{(l)}, x_j^{(k)}) \notin \tilde{\mathcal{E}}$ for $i \neq j$ or $l \neq k$, i.e. each node is only allowed to form an edge to instances of itself in another layer and not to another physical node in another layer. Furthermore, we enforce a fixed weight $\tilde{\mathbf{A}}_{lk} \geq 0$ for each layer-layer pair and collect these weights in the matrix $\tilde{\mathbf{A}} \in \mathbb{R}^{L \times L}$. We can then define the *inter-layer adjacency matrix* $\mathbf{A}_{\text{inter}} \in \mathbb{R}^{nL \times nL}$ by

$$\mathbf{A}_{\text{inter}} = \tilde{\mathbf{A}} \otimes \mathbf{I},$$

where $\mathbf{I} \in \mathbb{R}^{n \times n}$ and \otimes denotes the Kronecker product. Note that self-edges can be excluded by setting $\tilde{\mathbf{A}}_{ll} = 0$ for all $l = 1, \dots, L$.

We then define the *supra-adjacency matrix* $\mathbf{A} \in \mathbb{R}^{nL \times nL}$ as the weighted sum of the intra- and inter-layer adjacency matrices, where the parameter $\omega \in \mathbb{R}_{\geq 0}$ allows to control the relative importance of both adjacency matrices, i.e. both types of edges

$$\begin{aligned} \mathbf{A} &= \mathbf{A}_{\text{intra}} + \omega \mathbf{A}_{\text{inter}} = \text{blkdiag}[\mathbf{A}^{(1)}, \dots, \mathbf{A}^{(L)}] + \omega \tilde{\mathbf{A}} \otimes \mathbf{I} \\ &= \begin{bmatrix} \mathbf{A}^{(1)} & \mathbf{0} & \dots & \mathbf{0} \\ \mathbf{0} & \mathbf{A}^{(2)} & \dots & \mathbf{0} \\ \vdots & \vdots & \ddots & \vdots \\ \mathbf{0} & \mathbf{0} & \dots & \mathbf{A}^{(L)} \end{bmatrix} + \omega \begin{bmatrix} \tilde{\mathbf{A}}_{11}\mathbf{I} & \tilde{\mathbf{A}}_{12}\mathbf{I} & \dots & \tilde{\mathbf{A}}_{1L}\mathbf{I} \\ \tilde{\mathbf{A}}_{21}\mathbf{I} & \tilde{\mathbf{A}}_{22}\mathbf{I} & \dots & \tilde{\mathbf{A}}_{2L}\mathbf{I} \\ \vdots & \vdots & \ddots & \vdots \\ \tilde{\mathbf{A}}_{L1}\mathbf{I} & \tilde{\mathbf{A}}_{L2}\mathbf{I} & \dots & \tilde{\mathbf{A}}_{LL}\mathbf{I} \end{bmatrix}. \end{aligned} \quad (2.2)$$

Note that because of the special structure of Equation (2.2) we do not require to explicitly form the matrix \mathbf{A} , which is fully determined by the entries of the matrices $\mathbf{A}^{(1)}, \dots, \mathbf{A}^{(L)}$ and $\tilde{\mathbf{A}}$. As the numerical methods presented in this paper will only require the action of \mathbf{A} on vectors $\mathbf{v} \in \mathbb{R}^{nL}$, suitable functions can be implemented which realize the matrix-vector products $\mathbf{A}\mathbf{v}$ when only $\mathbf{A}^{(1)}, \dots, \mathbf{A}^{(L)}$ and $\tilde{\mathbf{A}}$

are available. Especially when n is large the memory requirement can be drastically reduced by this procedure.

We will be interested in applying *matrix functions* to the supra-adjacency matrix defined in Equation (2.2). There are several different definitions of matrix functions which are equivalent under certain conditions [35]. In the special case of real symmetric square matrices, [35, Definition 1.2] reads

$$f(\mathbf{A}) = \Phi f(\Lambda) \Phi^T, \quad (2.3)$$

with the eigendecomposition $\mathbf{A} = \Phi \Lambda \Phi^T$ where $\Phi \in \mathbb{R}^{nL \times nL}$ contains the orthonormal eigenvectors of \mathbf{A} and $\Lambda \in \mathbb{R}^{nL \times nL}$ is a diagonal matrix with the eigenvalues of \mathbf{A} on the diagonal. Thus in this case the matrix function only acts on the spectrum of \mathbf{A} and we require the real function f to be defined on this spectrum. Equation (2.3) applies to the supra-adjacency matrix in Equation (2.2) when all intra- and inter-layer edges are undirected in which case we have $\mathbf{A}_{\text{intra}} = \mathbf{A}_{\text{intra}}^T$ and $\mathbf{A}_{\text{inter}} = \mathbf{A}_{\text{inter}}^T$ and subsequently $\mathbf{A} = \mathbf{A}^T$. If we have at least one directed edge in the multilayer network other definitions may have to be used depending on whether \mathbf{A} is still diagonalizable. We present more details about the matrix function definitions and their numerical implementations in Section 5. The following section will show how the application of certain matrix functions can be used to determine the centrality of nodes in a given network.

3. Matrix function-based centrality measures

We introduce several centrality measures that are based on the application of the matrix exponential or the matrix resolvent function to the adjacency matrix of a network. These centrality measures have gained a lot of attention for their application to single-layer networks in recent years, cf. [9, 22, 23, 36] as well as the review article [8]. All measures can be motivated by considering walks along the edges of the network and they can be used to identify the network's most important nodes. In this section we restrict our discussion to the case of single-layer networks, cf. Figure 1a. In this situation, $\mathbf{A} = \mathbf{A}^{(1)}$ corresponds to the single graph layer's intra-layer adjacency matrix and there are no inter-layer edges present. In terms of notation we thus drop the superscript (l) indicating the layer ID for all related quantities throughout this section. Furthermore, we assume \mathbf{A} to represent an unweighted and undirected graph and discuss the differences in the weighted as well as the directed case at the end of this section.

We motivate the use of matrix functions by considering matrix powers of the adjacency matrix $\mathbf{A} \in \mathbb{R}^{n \times n}$ of a single-layer graph $\mathcal{G} = (\mathcal{V}, \mathcal{E})$ with $|V| = n$. It is well-known from graph theory that for an unweighted and undirected graph the entry $[\mathbf{A}^k]_{ij}$ denotes the number of walks of length k existing between nodes x_i and x_j [20]. A walk of length k is defined by a sequence of k adjacent nodes which may contain repeated nodes, i.e. we allow backtracking walks. For non-backtracking walks we refer the reader to [1, 4, 5]. In the special case $i = j$, we speak of closed walks that start and end at node x_i . These entries correspond to the diagonal elements of the adjacency matrix powers.

This notion enables us to easily express well-known network properties in terms of entries of the powers of the adjacency matrix. We can, for instance, write the *clustering coefficient* introduced in [55], which denotes the ratio of present and possible triangles (closed walks of length $k = 3$) around node x_i as

$$C(x_i) = \frac{2[\mathbf{A}^3]_{ii}}{d_i(d_i - 1)}, \quad i = 1, \dots, n,$$

where $d_i = \sum_{j=1}^n w(x_i, x_j)$ denotes the degree of node x_i .

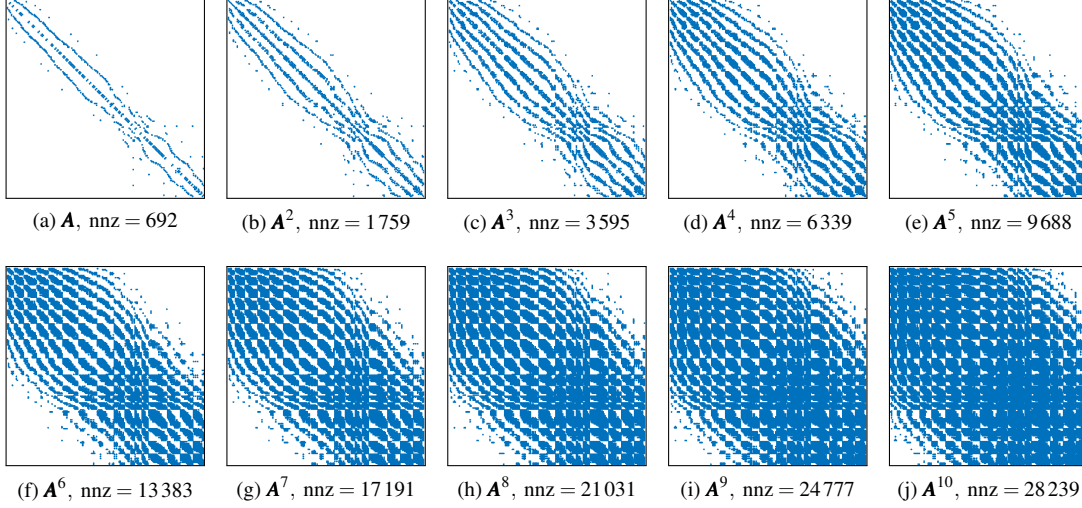


FIG. 2. Sparsity structure of the first ten adjacency matrix powers $\mathbf{A}, \dots, \mathbf{A}^{10}$ for a connected undirected single-layer graph with $n = 199$. The expression nnz denotes the number of non-zeros in the respective matrix power $\mathbf{A}^k \in \mathbb{R}^{199 \times 199}$.

Classical centrality measures like degree or eigenvector centrality can also be expressed in terms of the adjacency matrix. Degree centrality, which ranks each node based on its degree d_i can be written as $d_i = \mathbf{e}_i^T \mathbf{A} \mathbf{1}$ where $\mathbf{e}_i \in \mathbb{R}^n$ denotes the i th unit vector and $\mathbf{1} = [1, \dots, 1]^T \in \mathbb{R}^n$ the one vector.

Eigenvector centrality, which was first introduced in [15] and received a lot of attention for Google's PageRank eigenvector [16, 45], can also be related to powers of the graph's adjacency matrix. It is defined by the entries of the eigenvector ϕ corresponding to the largest eigenvalue λ_{\max} of \mathbf{A} . It can be obtained by a power iteration approximating the limit $\lim_{k \rightarrow \infty} \mathbf{A}^k \mathbf{v}$ unless the starting vector of the iteration is orthogonal to the sought eigenvector or the sought eigenvector is not unique, which is the case for graphs that are not connected. A graph is called connected if a walk is present between any pair of nodes.

Figure 2 illustrates the sparsity structure of the adjacency matrix powers $\mathbf{A}, \dots, \mathbf{A}^{10}$ for a connected undirected single-layer graph with $n = 199$ nodes. The smallest power K for which $\sum_{k=1}^K \mathbf{A}^k$ contains no zero entry is called the *diameter* of a connected network. It denotes the maximum distance of two vertices in the network, i.e. starting from an arbitrary node, every other node in the network can be reached by a walk of at most length K .

The concept of matrix function-based centrality measures allows to interpolate between degree centrality, which only considers walks of length one (i.e. only the matrix \mathbf{A}), and eigenvector centrality, which describes the stationary situation where the length of the walks goes to infinity (represented by \mathbf{A}^k for $k \rightarrow \infty$ in the power iteration). It has been shown in [12] that in fact degree and eigenvector centrality are limit cases of matrix function-based centrality measures. To this end, walks of all lengths are considered. As for most graphs the magnitude of the entries of the powers \mathbf{A}^k of the adjacency matrix grows rapidly as a function of k , one introduces a damping parameter that depends on k .

Two choices for such a damping parameter are usually considered. We will demonstrate that the factor $1/k!$, with $!$ denoting the factorial, leads to the exponential function and the factor α^k leads to the

resolvent function. In case of choosing the damping factor $1/k!$, we obtain the power series

$$\sum_{k=1}^{\infty} \frac{1}{k!} \mathbf{A}^k = \mathbf{A} + \frac{1}{2} \mathbf{A}^2 + \frac{1}{3!} \mathbf{A}^3 + \dots$$

Adding the term $k = 0$ does not change the node's ranking in our later definition of the centrality measures (it simply adds the value of one to each node's centrality value) and hence we obtain the power series of the matrix exponential

$$\sum_{k=0}^{\infty} \frac{1}{k!} \mathbf{A}^k = \mathbf{I} + \mathbf{A} + \frac{1}{2} \mathbf{A}^2 + \frac{1}{3!} \mathbf{A}^3 + \dots = e^{\mathbf{A}}.$$

Furthermore, one usually introduces an additional damping parameter β^k , which one chooses depending on the spectrum of \mathbf{A} to control the magnitude of the entries of the matrix function so that we get

$$\sum_{k=0}^{\infty} \frac{\beta^k}{k!} \mathbf{A}^k = \mathbf{I} + \beta \mathbf{A} + \frac{\beta^2}{2} \mathbf{A}^2 + \frac{\beta^3}{3!} \mathbf{A}^3 + \dots = e^{\beta \mathbf{A}}. \quad (3.1)$$

The matrix function from Equation (3.1) has been used to define several centrality and communicability measures for single-layer graphs. *Subgraph centrality*, which was first introduced in [23], is defined as the diagonal elements of $e^{\beta \mathbf{A}}$ and we write

$$SC(i, \beta) = \left[\mathbf{I} + \beta \mathbf{A} + \frac{\beta^2}{2} \mathbf{A}^2 + \frac{\beta^3}{3!} \mathbf{A}^3 + \dots \right]_{ii} = [e^{\beta \mathbf{A}}]_{ii} = \mathbf{e}_i^T e^{\beta \mathbf{A}} \mathbf{e}_i. \quad (3.2)$$

Sorting the nodes in descending order of their subgraph centrality value $SC(i, \beta)$ yields a ranking of the graph's nodes in terms of their centrality in the network.

The closely related *Estrada index* was introduced in [19] in the context of protein networks. It denotes a scalar measure for the total connectivity of a network where the subgraph centrality of all nodes in the network is summed up, i.e.,

$$EI(\mathcal{G}, \beta) = \sum_{i=1}^n SC(i, \beta) = \sum_{i=1}^n [e^{\beta \mathbf{A}}]_{ii} = \text{Tr}(e^{\beta \mathbf{A}}) = \sum_{i=1}^n e^{\beta \lambda_i}, \quad (3.3)$$

where $\text{Tr}(\mathbf{A}) = \sum_{i=1}^n \mathbf{A}_{ii}$ denotes the trace of a matrix and λ_i the i th eigenvalue of \mathbf{A} . Note that the last equality does not hold for non-diagonalizable matrices \mathbf{A} , which can be the case for directed networks.

The off-diagonal elements of $e^{\beta \mathbf{A}}$ can be used to measure the *communicability* between two nodes x_i and x_j [8]. We define

$$C(i, j, \beta) = [e^{\beta \mathbf{A}}]_{ij} = \mathbf{e}_i^T e^{\beta \mathbf{A}} \mathbf{e}_j. \quad (3.4)$$

Furthermore, the importance of a node x_i in the flow of information in a network can be expressed by the *total communicability* [11] defined as

$$TC(i, \beta) = [e^{\beta \mathbf{A}} \mathbf{1}]_i = \mathbf{e}_i^T e^{\beta \mathbf{A}} \mathbf{1}. \quad (3.5)$$

Similarly to the Estrada index the *total network communicability* [11] defines another scalar measure for the connectivity of the full network by averaging over all communicabilities in the network

$$TNC(\mathcal{G}) = \frac{1}{n} \sum_{i=1}^n \sum_{j=1}^n [e^{\beta \mathbf{A}}]_{ij} = \frac{1}{n} \mathbf{1}^T e^{\beta \mathbf{A}} \mathbf{1}.$$

As the weighting factor $1/k!$ decreases rapidly with growing k , longer walks may be underrepresented in certain applications. An alternative weighting with a parameter α^k leads to the power series of the matrix resolvent function

$$\sum_{k=0}^{\infty} \alpha^k \mathbf{A}^k = \mathbf{I} + \alpha \mathbf{A} + \alpha^2 \mathbf{A}^2 + \dots = (\mathbf{I} - \alpha \mathbf{A})^{-1}.$$

We choose the parameter α such that it satisfies $0 < \alpha < 1/\lambda_{\max}$. This choice guarantees that all derivatives $f^{(j)}(x)$, $j = 1, 2, \dots$ of the resolvent function $f(x) = \frac{1}{1-\alpha x}$ are strictly positive for $x \in [\lambda_{\min}, \lambda_{\max}]$ for λ_{\min} the smallest eigenvalue of \mathbf{A} , which will be required to obtain quadrature bounds in Section 5.2.

Similar to subgraph centrality we can now define the *resolvent-based subgraph centrality* [8] as the diagonal elements of the matrix resolvent function

$$SC_{\text{res}}(i, \alpha) = [\mathbf{I} + \alpha \mathbf{A} + \alpha^2 \mathbf{A}^2 + \dots]_{ii} = [(\mathbf{I} - \alpha \mathbf{A})^{-1}]_{ii} = \mathbf{e}_i^T (\mathbf{I} - \alpha \mathbf{A})^{-1} \mathbf{e}_i.$$

A very similar construction to the total communicability involving the matrix resolvent function was already introduced decades earlier by Katz [36]. The so-called *Katz centrality* is defined as

$$KC(i, \alpha) = [(\mathbf{I} - \alpha \mathbf{A})^{-1} \mathbf{1}]_i = \mathbf{e}_i^T (\mathbf{I} - \alpha \mathbf{A})^{-1} \mathbf{1}. \quad (3.6)$$

We remark that all above centrality measures may be evaluated by either computing an expression of the form $f(\mathbf{A})\mathbf{b}$ or $\mathbf{u}^T f(\mathbf{A})\mathbf{v}$. Quantities of the form $\mathbf{e}_i^T f(\mathbf{A})\mathbf{1}$ only require the evaluation of $f(\mathbf{A})\mathbf{1}$ once. The resulting vector contains the centrality of node x_i in the i th entry of $f(\mathbf{A})\mathbf{1}$ for all $i = 1, \dots, n$. Note that all measures of the form $\mathbf{u}^T f(\mathbf{A})\mathbf{v}$ except for the communicability $C(i, j, \beta)$ simplify further due to the fact that $\mathbf{u} = \mathbf{v}$. We give an overview of all introduced matrix function-based centrality measures in Table 1 categorized into the above-mentioned more general expressions.

The motivation we used for introducing matrix function-based centrality measures by means of adjacency matrix powers makes *Krylov subspace methods* an intuitive tool for the evaluation of the involved matrix function expressions. Here, approximations for quantities $f(\mathbf{A})\mathbf{v}$ using the Krylov subspace

$$\mathcal{K}_k(\mathbf{A}, \mathbf{v}) = \text{span}\{\mathbf{v}, \mathbf{A}\mathbf{v}, \mathbf{A}^2\mathbf{v}, \dots, \mathbf{A}^{k-1}\mathbf{v}\}$$

can be interpreted as approximating f by a matrix polynomial of degree $k-1$ [8]. Section 5 gives details about the numerical treatment of the different expressions.

In the case of weighted adjacency matrices, the entries in $[\mathbf{A}^k]_{ij}$ can no longer be interpreted as the number of walks of length k between nodes x_i and x_j . However, formally all above definitions equally apply and the elements of the matrix powers still contain information about the relative connectivity of pairs of nodes. In certain applications, these entries could, e.g., denote the number of people that are transported from one place to another or the number of messages transferred from one individual to another.

In the case of directed networks we are faced with nonsymmetric adjacency matrices \mathbf{A} , i.e. the presence of an edge pointing from node x_i to x_j does not guarantee that an edge pointing from node x_j to x_i exists. In the case of weighted directed graphs both edges might exist but carry different weights. Subsequently all matrix powers \mathbf{A}^k are in general also nonsymmetric. Thus, we need to differentiate between each node's role as a broadcaster and a receiver. Nodes with a high *broadcaster centrality* are called *hubs* and are characterized by a large amount of outward flow. Likewise, nodes with a high *receiver centrality* are called *authorities* and are characterized by a large amount of inward flow.

$f(\mathbf{A})\mathbf{b}$	$\mathbf{u}^T f(\mathbf{A})\mathbf{u}$	$\mathbf{u}^T f(\mathbf{A})\mathbf{v}$
Total communicability $TC(i, \beta) = \mathbf{e}_i^T \mathbf{e}^{\beta \mathbf{A}} \mathbf{1}$ Katz centrality $KC(i, \alpha) = \mathbf{e}_i^T (\mathbf{I} - \alpha \mathbf{A})^{-1} \mathbf{1}$	Subgraph centrality $SC(i, \beta) = \mathbf{e}_i^T \mathbf{e}^{\beta \mathbf{A}} \mathbf{e}_i$ Resolvent-based subgraph centrality $SC_{\text{res}}(i, \alpha) = \mathbf{e}_i^T (\mathbf{I} - \alpha \mathbf{A})^{-1} \mathbf{e}_i$ Estrada index $EI(\mathcal{G}, \beta) = \sum_{i=1}^{nL} \mathbf{e}_i^T \mathbf{e}^{\beta \mathbf{A}} \mathbf{e}_i$ Total network communicability $TNC(\mathcal{G}) = \frac{1}{nL} \mathbf{1}^T \mathbf{e}^{\beta \mathbf{A}} \mathbf{1}$	Communicability $C(i, j, \beta) = \mathbf{e}_i^T \mathbf{e}^{\beta \mathbf{A}} \mathbf{e}_j$

Table 1. Overview of all defined matrix function-based centrality measures categorized into more general matrix function expressions. Note that throughout Section 3 we have assumed $L = 1$.

In degree centrality, broadcaster centrality is given by each node's out-degree, i.e. $\mathbf{e}_i^T \mathbf{A} \mathbf{1}$. Receiver degree centrality is defined via the network's in-degrees, which are obtained via $\mathbf{e}_i^T \mathbf{A}^T \mathbf{1}$.

In eigenvector centrality, broadcaster centralities are given by the entries of the right eigenvector ϕ to the largest eigenvalue λ_{\max} that satisfies $\mathbf{A}\phi = \lambda_{\max}\phi$. Receiver centralities are given by the entries of the left eigenvector ψ to the largest eigenvalue μ_{\max} that satisfies $\psi^T \mathbf{A} = \mu_{\max} \psi^T \Leftrightarrow \mathbf{A}^T \psi = \mu_{\max} \psi$.

For matrix function-based centrality measures we must now also take care of the fact that in general $\mathbf{A}^k \neq (\mathbf{A}^k)^T$ for all $k = 1, 2, \dots$. Similarly to the case of degree and eigenvector centrality we obtain broadcaster matrix function centralities by considering the above definitions and receiver centralities by replacing $f(\mathbf{A})$ by $f(\mathbf{A}^T)$ [8]. However, subgraph centrality and resolvent-based subgraph centrality, which are defined as the diagonal elements $[f(\mathbf{A})]_{ii}$, can not differentiate between broadcaster and receiver centrality as by [35, Theorem 1.13(b)] we have $f(\mathbf{A}^T) = f(\mathbf{A})^T$ and thus we see that for the diagonal entries $[f(\mathbf{A})]_{ii} = [f(\mathbf{A}^T)]_{ii}$ for all $i = 1, \dots, n$. In this case, we can instead consider the undirected bipartite graph representation of a directed graph [8] by defining

$$\mathcal{A} = \begin{bmatrix} \mathbf{0} & \mathbf{A} \\ \mathbf{A}^T & \mathbf{0} \end{bmatrix} \in \mathbb{R}^{2n \times 2n}, \quad (3.7)$$

and obtain broadcaster centralities as $[f(\mathcal{A})]_{ii}$ for $i = 1, \dots, n$ and receiver centralities as $[f(\mathcal{A})]_{ii}$ for $i = n+1, \dots, 2n$ for both $f(\mathcal{A}) = e^{\beta \mathcal{A}}$ and $f(\mathcal{A}) = (\mathbf{I} - \alpha \mathcal{A})^{-1}$.

4. Definition of matrix function-based multilayer centrality measures

We now generalize the matrix function-based centrality measures introduced for the single-layer case in Section 3 to the situation of layer-coupled multiplex networks. To this end, we return to the multilayer graph representation specified in Section 2 in which each vertex $x_i^{(l)}$ represents a node-layer pair, i.e. the instance of physical node x_i in layer l , and apply the matrix function-based centrality measures from Section 3 to the corresponding supra-adjacency matrix defined in Equation (2.2). This approach yields centrality values for all node-layer pairs, which we denote by the term *joint centralities* that was introduced in [51]. Consequently, we add layer indices to all quantities in Table 1, e.g. $TC(i, l, \beta)$ or $C(i, l, j, k, \beta)$. Note that all quantities also depend on the parameter value ω , which trades off the relative importance of intra- and inter-layer edge weights. However, we do not explicitly include this dependency in the notation. Furthermore, we introduce the aggregated *marginal* and *conditional*

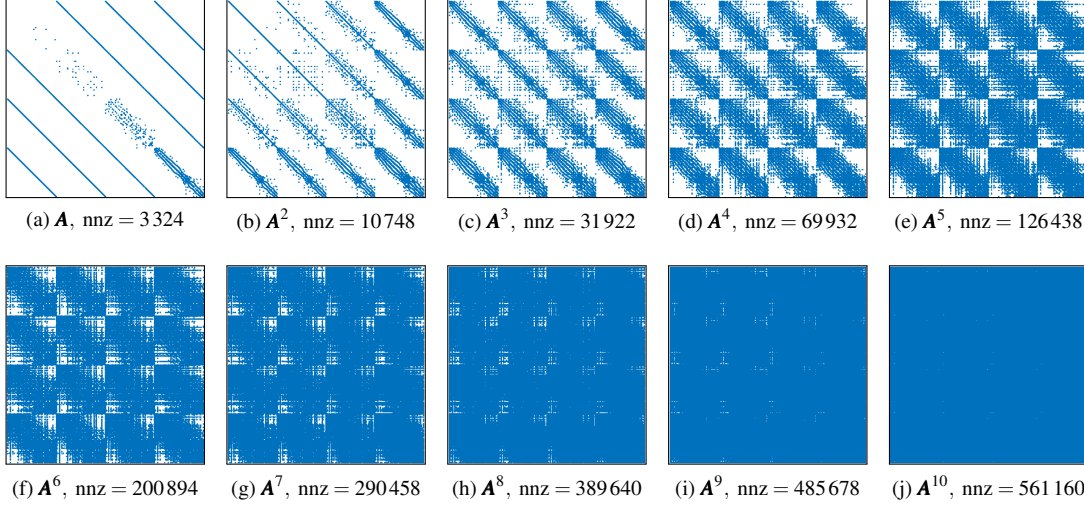


FIG. 3. Sparsity structure of the first ten adjacency matrix powers $\mathbf{A}, \dots, \mathbf{A}^{10}$ of an undirected layer-coupled multiplex network with $n = 199$ and $L = 4$ as well as all-to-all inter-layer coupling without self-edges. Layer four in the bottom right block corresponds to the single-layer adjacency matrix from Figure 2. The expression nnz denotes the number of non-zeros in the respective matrix power $\mathbf{A}^k \in \mathbb{R}^{796 \times 796}$.

centralities [51].

Within the framework of layer-coupled multiplex networks, the interpretation of the single-layer adjacency matrix in terms of walks along edges of the network naturally carries over to the supra-adjacency matrix from Equation (2.2). For temporal networks dynamical networks may be a more suitable network modeling approach and we comment on this at the end of this section. In the remaining cases, one step of a walk on a multilayer network starting from node $x_i^{(l)}$ can either follow an intra-layer edge towards $x_j^{(l)}$ within the same layer or an inter-layer edge towards $x_i^{(k)}$ in another layer, given that at least one such edge exists for $i \neq j$ or $l \neq k$, respectively. As already mentioned in Section 2, several inter-layer coupling matrices $\tilde{\mathbf{A}} \in \mathbb{R}^{L \times L}$ can be used to create meaningful multilayer graphs from multiple node-aligned single-layer graphs if no inter-layer coupling weights are specified by the data. Prominent examples include all-to-all coupling [53] with and without self-edges, which can be represented by the inter-layer weight matrices $\tilde{\mathbf{A}} = \mathbf{1}\mathbf{1}^T$ and $\tilde{\mathbf{A}} = \mathbf{1}\mathbf{1}^T - \mathbf{I}$, respectively. Temporal inter-layer coupling, which requires a notion of order among the layers, can, by our approach, be modeled by an inter-layer weight matrix $\tilde{\mathbf{A}}$, which is non-zero on both subdiagonals and zero otherwise in the undirected case and by an $\tilde{\mathbf{A}}$, which is non-zero on one subdiagonal and zero otherwise in the directed case [51].

Figure 3 illustrates the sparsity structure of the matrix powers $\mathbf{A}, \dots, \mathbf{A}^{10}$ of an undirected layer-coupled multiplex network with $n = 199$ nodes and $L = 4$ layers and all-to-all inter-layer coupling without self-edges, i.e. $\tilde{\mathbf{A}} = \mathbf{1}\mathbf{1}^T - \mathbf{I} \in \mathbb{R}^{4 \times 4}$. By [53, Theorem 3.7] \mathbf{A} represents a connected multilayer graph as both $\mathbf{A}^{(4)}$ and $\tilde{\mathbf{A}}$ are irreducible matrices. Note that layer four in the bottom right block corresponds to the single-layer adjacency matrix from Figure 2 but the relative number of non-zeros in the matrix powers \mathbf{A}^k increases more rapidly than in the single-layer case due to the high degree of connectivity of the inter-layer coupling. Applying the matrix function-based centrality measures from Section 3 to the

supra-adjacency matrix from Equation (2.2) yields centrality values for all node-layer pairs of the layer-coupled multiplex network. This allows us to rank the node-layer pairs in terms of their centrality in the network and to identify the most central node-layer pairs. Following [51] we call the resulting centrality value of $x_i^{(l)}$ the *joint centrality* $JC(i, l)$ of the node-layer pair (i, l) and also introduce aggregated *marginal* as well as *conditional centralities*.

The concept of *marginal node centrality* $MNC(i)$ denotes the importance of a physical node x_i by summing up the centrality values of its instances across all layers, i.e.

$$MNC(i) = \sum_{l=1}^L JC(i, l). \quad (4.1)$$

Similarly, *marginal layer centrality* $MLC(l)$ denotes the importance of layer l by summing up the centrality values of all nodes in this layer, i.e.

$$MLC(l) = \sum_{i=1}^n JC(i, l). \quad (4.2)$$

Marginal centralities can thus be used to ascertain rankings of the centrality of physical nodes and layers across the full multilayer network.

In addition, the *conditional node centrality* $CNC(i, l)$ of the node-layer pair (i, l) conditioned on the physical node x_i denotes the relative importance of the node-layer pair (i, l) across all instances of x_i and is defined as

$$CNC(i, l) = JC(i, l) / MNC(i). \quad (4.3)$$

Similarly, the *conditional layer centrality* $CLC(i, l)$ of the node-layer pair (i, l) conditioned on layer l denotes the relative importance of the node-layer pair (i, l) in comparison to all other nodes in layer l and is defined as

$$CLC(i, l) = JC(i, l) / MLC(l). \quad (4.4)$$

Conditional centralities thus yield the relative importance of node-layer pairs compared to either all instances of the same physical node or to all node-layer pairs from the same layer.

Note, however, that the above aggregation techniques may not establish the desired interpretability for temporal multilayer networks. In this situation one is faced with an ordered sequence of layers, which may describe the change of one feature or one type of relationship between the entities over time. As the above aggregated centralities then perform an averaging over time, these measures usually fail to capture the temporal dynamics of the network, i.e. changes of connectivity or relationships over time. A possible remedy could be the application and comparison of the centrality measures for subsets of temporal layers representing different time intervals. Alternatively, dynamic networks have proven to be a useful tool and we refer the reader to [6, 8, 18, 33].

5. Efficient methods for computing multilayer centrality measures

This section presents efficient numerical methods for the evaluation of certain matrix function expressions, which arise in matrix function-based centrality measures. While all methods are applicable to any real square matrix \mathbf{A} , we are particularly interested in the case where \mathbf{A} represents the supra-adjacency matrix of a layer-coupled multiplex network. Under the assumption of sparsity in the supra-adjacency matrix all presented methods scale linearly in the number of node-layer pairs of the network which allows the rapid treatment of large networks with the number of node-layer pairs at least in the millions.

quantity	$f(\mathbf{A})\mathbf{b}$	$\mathbf{u}^T f(\mathbf{A})\mathbf{v}$ and $\mathbf{u}^T f(\mathbf{A})\mathbf{u}$
$\mathbf{A} = \mathbf{A}^T$	Lanczos, Section 5.1	Lanczos & Gauss quadrature, Section 5.2.1
$\mathbf{A} \neq \mathbf{A}^T$	Arnoldi, Section 5.1	Lanczos on Equation (3.7) & quadrature, Arnoldi with shifted right vector, nonsym. block Lanczos & quadrature, Section 5.2.2

Table 2. Summary of the proposed numerical methods to compute the different types of centrality measures for symmetric and nonsymmetric supra-adjacency matrices \mathbf{A} .

However, some measures require the evaluation of a separate matrix function expression for each node-layer pair, which can become computationally infeasible for large-scale networks. In these cases it is still possible to compute centralities for selected node-layer pairs, cf. Section 5.2.

We differentiate between two types of centrality measures as well as symmetric and nonsymmetric supra-adjacency matrices. We summarize the proposed numerical methods for the different cases in Table 2. Note that many of the numerical methods in this section as well as some additional methods have been summarized in [8] in the context of single-layer networks.

5.1 Centrality measures based on the evaluation of $f(\mathbf{A})\mathbf{b}$

In this section we show how to efficiently compute quantities of the form $f(\mathbf{A})\mathbf{b}$ using *Krylov subspace methods* for $\mathbf{A} \in \mathbb{R}^{nL \times nL}$, $\mathbf{b} \in \mathbb{R}^{nL}$, and the scalar function f defined on the spectrum of \mathbf{A} [31, 35]. This enables the approximation of the total communicability from Equation (3.5) as well as Katz centrality from Equation (3.6) using the *symmetric Lanczos method* [39] in the symmetric case and the *Arnoldi method* [3] in the nonsymmetric case. Both centrality measures can be computed rapidly: the symmetric case requires only one evaluation of $f(\mathbf{A})\mathbf{1}$ and the nonsymmetric case requires the two evaluations $f(\mathbf{A})\mathbf{1}$ and $f(\mathbf{A}^T)\mathbf{1}$ for broadcaster and receiver centralities, respectively. The resulting vector then contains the joint centralities of all node-layer pairs, cf. the discussion at the end of Section 3. Under the assumption of sparse supra-adjacency matrices where the computational complexity of matrix-vector products can be assumed to be $\mathcal{O}(nL)$, both total communicability and Katz centrality also scale linearly in the number of node-layer pairs of the network as the matrix-vector products represent the computational bottleneck in both the symmetric Lanczos and Arnoldi's method. In this light, the limiting factor for the maximally computable network size for these measures is likely to be limited by the memory required to store the supra-adjacency matrix.

Both the symmetric Lanczos and the Arnoldi method construct the k th column of an orthonormal basis $\mathbf{Q}_k \in \mathbb{R}^{nL \times k}$ of the Krylov subspace

$$\mathcal{K}_k(\mathbf{A}, \mathbf{v}) = \text{span}\{\mathbf{v}, \mathbf{A}\mathbf{v}, \mathbf{A}^2\mathbf{v}, \dots, \mathbf{A}^{k-1}\mathbf{v}\}$$

of the matrix $\mathbf{A} \in \mathbb{R}^{nL \times nL}$ and an initial vector $\mathbf{v} \in \mathbb{R}^{nL}$ in the k th step of the respective method. In the nonsymmetric case $\mathbf{A} \neq \mathbf{A}^T$ these basis vectors approximate \mathbf{A} via $\mathbf{A} \approx \mathbf{Q}_k \mathbf{H}_k \mathbf{Q}_k^T$ where $\mathbf{H}_k \in \mathbb{R}^{k \times k}$ has Hessenberg form. In the symmetric case $\mathbf{A} = \mathbf{A}^T$ this approximation simplifies to $\mathbf{A} \approx \mathbf{Q}_k \mathbf{T}_k \mathbf{Q}_k^T$ with $\mathbf{T}_k \in \mathbb{R}^{k \times k}$ tridiagonal. In exact arithmetic both approximations are exact for $k \geq m$, where m is the degree of the minimal polynomial of \mathbf{A} with respect to \mathbf{v} [47]. In practice, however, good approximations are often obtained after $k \ll nL$ steps of the respective method. More details on the algorithms as well as many practical aspects of efficient and stable implementations including restarts for both methods can be found in [31, 47].

Having obtained the decomposition $\mathbf{A} \approx \mathbf{Q}_k \mathbf{H}_k \mathbf{Q}_k^T$ in the nonsymmetric case, an approximation of the quantity $f(\mathbf{A})\mathbf{b}$ is given by [35]

$$f(\mathbf{A})\mathbf{b} \approx \mathbf{Q}_k f(\mathbf{H}_k) \mathbf{Q}_k^T \mathbf{b}. \quad (5.1)$$

The explicit evaluation of $f(\mathbf{H}_k) \in \mathbb{R}^{k \times k}$ can be obtained rapidly by well-established methods in the case of both the matrix exponential [42] and the matrix resolvent function where a small regular $k \times k$ linear system needs to be solved. We remark again that in this case $f(\mathbf{A})\mathbf{b}$ yields broadcaster and $f(\mathbf{A}^T)\mathbf{b}$ yields receiver centralities or communicabilities, respectively, for all node-layer pairs.

For undirected networks where $\mathbf{A} = \mathbf{A}^T$, Equation (5.1) holds with $\mathbf{H}_k = \mathbf{T}_k$. In this case one can, e.g., compute the eigendecomposition $\mathbf{T}_k = \mathbf{S}_k \mathbf{\Theta}_k \mathbf{S}_k^T$ with $\mathbf{S}_k \in \mathbb{R}^{k \times k}$ containing the eigenvectors and the diagonal matrix $\mathbf{\Theta}_k \in \mathbb{R}^{k \times k}$ the eigenvalues of \mathbf{T}_k and approximate the desired quantities via

$$f(\mathbf{A})\mathbf{b} \approx \mathbf{Q}_k \mathbf{S}_k f(\mathbf{\Theta}_k) \mathbf{S}_k^T \mathbf{Q}_k^T \mathbf{b}, \quad (5.2)$$

where $f(\mathbf{\Theta}_k)$ applies f elementwise to the eigenvalues of \mathbf{T}_k [31, 35].

For the construction of \mathbf{Q}_k as well as the implementation of Equations (5.1) and (5.2) we rely on the `funm.kryl` toolbox [34], which supports restarted Lanczos and Arnoldi methods.

5.2 Centrality measures based on the evaluation of $\mathbf{u}^T f(\mathbf{A})\mathbf{u}$ and $\mathbf{u}^T f(\mathbf{A})\mathbf{v}$

This section presents numerical methods for the computation of subgraph centrality, the Estrada index, total network communicability, and the resolvent-based subgraph centrality, which can all be written in the form $\mathbf{u}^T f(\mathbf{A})\mathbf{u}$, cf. the center column of Table 1. We also briefly comment on the computation of the communicability $C(i, l, j, k, \beta)$, which is of the form $\mathbf{u}^T f(\mathbf{A})\mathbf{v}$. We use the well-known relation between Gauss quadrature, the symmetric Lanczos method, and orthogonal polynomials discussed by Golub and Meurant in [27–29, 32] for the computation of lower and upper bounds on these centrality measures in the case of symmetric supra-adjacency matrices, i.e. undirected networks. For nonsymmetric supra-adjacency matrices, i.e. directed networks, we encounter numerical stability issues of standard algorithms for our specific problems. To this end, we present three different approaches for this type of problem, namely the application of the symmetric Lanczos method to the symmetric bipartite graph representation of the directed network defined in Equation (3.7), the inclusion of a stabilizing shift to the right vector in Arnoldi's method, and the application of the nonsymmetric block Lanczos process in conjunction with Gauss and anti-Gauss quadrature rules [24].

Except for the total network communicability and unlike the measures considered in Section 5.1 all centrality measures covered in this section require the evaluation of a separate matrix function expression $\mathbf{u}^T f(\mathbf{A})\mathbf{u}$ for each node-layer pair¹. Using the same argument as in the previous section this leads to a computational complexity of $\mathcal{O}(nL)$ to compute one node-layer pair's centrality. Of course, this complexity increases to $\mathcal{O}(n^2 L^2)$ when the centrality values of all nL node-layer pairs are required. Unfortunately, this makes the computation of all expressions $\mathbf{u}^T f(\mathbf{A})\mathbf{u}$ infeasible for large-scale networks. A possible approach could be to preselect the r most important node-layer pairs of a measure of the form $f(\mathbf{A})\mathbf{b}$ and compute the measure $\mathbf{u}^T f(\mathbf{A})\mathbf{u}$ only for this subset, which may have an acceptable computational complexity of $\mathcal{O}(rnL)$. However, numerical experiments in Section 6.4 indicate that this approach is unlikely to identify the top-ranked node-layer pairs of a given $\mathbf{e}_i^T f(\mathbf{A})\mathbf{e}_i$ measure for

¹The communicability $C(i, l, j, k, \beta)$ even requires the evaluation of a separate matrix function expression $\mathbf{u}^T f(\mathbf{A})\mathbf{v}$ for each pair of node-layer pairs which thus leads to a computational complexity of $\mathcal{O}(n^3 L^3)$.

large-scale networks. Here, it is observed that the similarity between rankings obtained by $f(\mathbf{A})\mathbf{1}$ and $\mathbf{e}_i^T f(\mathbf{A})\mathbf{e}_i$ even for the same matrix function tends to decrease as the size of the network and consequently the contribution of off-diagonal matrix function entries to quantities of the form $f(\mathbf{A})\mathbf{1}$ increases.

5.2.1 The symmetric case In order to find lower and upper bounds on quantities of the form $\mathbf{u}^T f(\mathbf{A})\mathbf{u}$ for $\mathbf{A} = \mathbf{A}^T \in \mathbb{R}^{nL \times nL}$, $\mathbf{u} \in \mathbb{R}^{nL}$, and f a smooth (possibly C^∞) function on a given interval on the real line we follow the *Gauss quadrature* approach by Golub and Meurant [27–29, 32] and consider

$$\mathbf{u}^T f(\mathbf{A})\mathbf{u} = \underbrace{\mathbf{u}^T \Phi}_{=: \mathbf{p}^T} f(\Lambda) \underbrace{\Phi^T \mathbf{u}}_{=: \mathbf{p}} = \mathbf{p}^T f(\Lambda) \mathbf{p} = \sum_{i=1}^{nL} f(\lambda_i) \mathbf{p}_i^2, \quad (5.3)$$

for $\mathbf{A} = \Phi \Lambda \Phi^T$ where $\Phi \in \mathbb{R}^{nL \times nL}$ contains the eigenvectors of \mathbf{A} and $\Lambda = \text{diag}[\lambda_1, \lambda_2, \dots, \lambda_{nL}]$ the eigenvalues $\lambda_{\min} = \lambda_1 \leq \lambda_2 \leq \dots \leq \lambda_{nL} = \lambda_{\max}$ of \mathbf{A} . Note that this eigendecomposition always exists for symmetric \mathbf{A} . Furthermore, Equation (5.3) can be written as the Riemann-Stieltjes integral

$$\mathbf{u}^T f(\mathbf{A})\mathbf{u} = \int_a^b f(\lambda) d\mu(\lambda) = \sum_{j=1}^k w_j f(t_j) + \sum_{m=1}^M v_m f(z_m) + R[f],$$

with the remainder $R[f]$, and with the weights $\{w_j\}_{j=1}^k$ at the k Gauss nodes $\{t_j\}_{j=1}^k$, the weights $\{v_m\}_{m=1}^M$ at the prescribed (interval boundary) nodes $\{z_m\}_{m=1}^M \subseteq \{a, b\}$, as well as the measure

$$\mu(\lambda) = \begin{cases} 0, & \lambda < a = \lambda_1, \\ \sum_{j=1}^i \mathbf{p}_j^2, & \lambda_i \leq \lambda < \lambda_{i+1}, \\ \sum_{j=1}^{nL} \mathbf{p}_j^2, & b = \lambda_{nL} \leq \lambda. \end{cases}$$

Now, using a beautiful relation between Gauss quadrature and orthogonal polynomials constructed from a three-term recurrence relation [27–29, 32] the Gauss nodes and weights do not have to be computed explicitly, but can be obtained from a tridiagonalization of the matrix \mathbf{A} , which can be constructed using the Lanczos process, cf. [39], [31, Section 10.1], and Section 5.1. Given the tridiagonal matrix \mathbf{T}_k after k Lanczos steps it can be shown [27, Theorem 3.4] that

$$\sum_{j=1}^k w_j f(t_j) = \mathbf{e}_1^T f(\mathbf{T}_k) \mathbf{e}_1,$$

with the unit vector $\mathbf{e}_1 \in \mathbb{R}^k$ where the eigendecomposition $\mathbf{T}_k = \mathbf{S}_k \Theta_k \mathbf{S}_k^T$ with Θ_k and \mathbf{S}_k the Ritz values and vectors of \mathbf{A} can be computed cheaply. We can then easily evaluate $f(\mathbf{T}_k) = \mathbf{S}_k f(\Theta_k) \mathbf{S}_k^T$ by elementwise application of f to the eigenvalues Θ_k . Alternatively, the Gauss nodes t_j are given by the eigenvalues of \mathbf{T}_k contained in Θ_k and the Gauss weights w_j are given by the first entries of the respective eigenvectors in \mathbf{S}_k .

This relation can be extended to yield *Gauss–Radau* and *Gauss–Lobatto* rules by prescribing the nodes z_m as eigenvalues to the matrix \mathbf{T}_k , cf. [27, Section 3.1] or [29, Section 6.2] for the details. As the exponential function $f(x) = e^{\beta x}$ and the resolvent function $f(x) = \frac{1}{1-\alpha x}$ with $0 < \alpha < 1/\lambda_{\max}$ as well as all their derivatives are strictly positive for $x \in [\lambda_{\min}, \lambda_{\max}]$ we can determine the sign of the remainder $R[f]$ for all quadrature rules. More specifically, we obtain lower bounds on $\mathbf{u}^T f(\mathbf{A})\mathbf{u}$ by the

Gauss rule and the Gauss–Radau rule with $z_m = \lambda_{\min}$ as well as upper bounds by the Gauss–Radau rule with $z_m = \lambda_{\max}$ and the Gauss–Lobatto rule.

The case $\mathbf{u}^T f(\mathbf{A}) \mathbf{v}$ with $\mathbf{u} \neq \mathbf{v}$ can be handled for $\mathbf{A} = \mathbf{A}^T$ using the above methods together with the polarization identity [29]

$$\mathbf{u}^T f(\mathbf{A}) \mathbf{v} = \frac{1}{4} [(\mathbf{u} + \mathbf{v})^T f(\mathbf{A})(\mathbf{u} + \mathbf{v}) - (\mathbf{u} - \mathbf{v})^T f(\mathbf{A})(\mathbf{u} - \mathbf{v})], \quad (5.4)$$

at the cost of the evaluation of two quantities of the form $\mathbf{u}^T f(\mathbf{A}) \mathbf{u}$.

5.2.2 The nonsymmetric case Trying to apply the above quadrature rules in the nonsymmetric case leads to several issues. In the following we discuss these issues as well as three different approaches to overcome them.

As $\mathbf{A} \neq \mathbf{A}^T$ is no longer guaranteed to be diagonalizable Equation (5.3) no longer holds. Instead, alternative approaches exist, which are based on the construction of bi-orthogonal polynomials, e.g. by the *nonsymmetric Lanczos method* [29, Section 6.5] or by the *biconjugate gradient method* (BiCG) [48] for Gauss quadrature in the complex plane. Unfortunately, among the quantities $\mathbf{u}^T f(\mathbf{A}) \mathbf{u}$ considered in this section only the total network communicability can reliably be computed by these methods. For the remaining quantities, due to the typically encountered sparsity of the supra-adjacency matrices in combination with the sparsity of the unit vectors as right vectors, we experience serious numerical stability issues with the above methods as well as the Arnoldi method applied only to $f(\mathbf{A}) \mathbf{u}$. It can, for instance, be shown that the nonsymmetric Lanczos method is guaranteed to encounter a serious breakdown in the first step when trying to compute either subgraph or resolvent-based subgraph centrality for isolated node-layer pairs in the respective intra-layer when the network additionally satisfies certain sparsity conditions in the inter-layer coupling. We dedicate the remainder of this section to the introduction of stable numerical methods for the computation of centrality measures of the form $\mathbf{e}_i^T f(\mathbf{A}) \mathbf{e}_i$.

The numerical stability issue described above has previously been discussed in [24]. The author’s solution is to first employ the *nonsymmetric block Lanczos method* with an additional sparse column in the block vector and then use Gauss and *anti-Gauss* quadrature rules to obtain bounds on the desired quantities. We choose this method as our *first approach* to evaluate quantities of the form $\mathbf{e}_i^T f(\mathbf{A}) \mathbf{e}_i$ in the nonsymmetric case and refer to [24] for the details. A pleasant side-effect of this method is that we also obtain certain off-diagonal matrix function entries, e.g. communicabilities, for free. While our own Matlab implementation of this approach runs stably for most inter-layer coupling matrices, we still encounter some serious breakdowns in the case of directed temporal inter-layer coupling in which the following two alternative approaches also succeed.

Our *second approach* concerns the Arnoldi method, which can be used to evaluate quantities of the form $\mathbf{u}^T f(\mathbf{A}) \mathbf{u}$ by applying it to the approximation of $\mathbf{y} := f(\mathbf{A}) \mathbf{u}$ in a first step and then obtain $\mathbf{u}^T f(\mathbf{A}) \mathbf{u} = \mathbf{u}^T \mathbf{y}$ in a second step. As this procedure exhibits similar stability issues for $\mathbf{u} = \mathbf{e}_i$ as the nonsymmetric Lanczos method and BiCG we propose to add a dense shift to the right vector $\mathbf{u} = \mathbf{e}_i$, e.g. the one vector $\mathbf{1}$. For subgraph and resolvent-based subgraph centrality this leads to

$$\mathbf{e}_i^T f(\mathbf{A}) \mathbf{e}_i = \mathbf{e}_i^T f(\mathbf{A})(\mathbf{e}_i + \mathbf{1}) - \mathbf{e}_i^T f(\mathbf{A}) \mathbf{1}. \quad (5.5)$$

Here the quantity $\mathbf{e}_i^T f(\mathbf{A}) \mathbf{1}$ corresponds to the total communicability in the case of the matrix exponential and to Katz centrality in the case of the matrix resolvent function and it can be evaluated by one application of Arnoldi’s method, cf. Section 5.1. The quantity $f(\mathbf{A})(\mathbf{e}_i + \mathbf{1})$ now contains a dense right vector for all $i = 1, \dots, nL$ and no longer suffers from the stability issue. Thus, we can evaluate the

desired quantities for all nL node-layer pairs by applying $(nL + 1)$ stable Arnoldi procedures. Note that this only allows to approximate $\mathbf{e}_i^T f(\mathbf{A}) \mathbf{e}_i$ and not to compute bounds for it. However, this approach exhibits an interesting error cancellation property in some situations which will be demonstrated in an example at the end of Section 6.2.

Both approaches presented so far still fail to differentiate each node-layer pairs different role as broadcaster and receiver. To this end, our *third approach* considers the symmetric bipartite graph representation, which exists for any directed graph [8] and which is given by the block supra-adjacency matrix

$$\mathcal{A} = \begin{bmatrix} \mathbf{0} & \mathbf{A} \\ \mathbf{A}^T & \mathbf{0} \end{bmatrix} \in \mathbb{R}^{2nL \times 2nL}. \quad (5.6)$$

Obviously, we have $\mathcal{A} = \mathcal{A}^T$ and thus we can employ the quadrature rules from Section 5.2.1 to compute bounds on quantities of the form $\mathbf{u}^T f(\mathcal{A}) \mathbf{u}$ and in particular $\mathbf{e}_i^T f(\mathcal{A}) \mathbf{e}_i$ with $\mathbf{e}_i \in \mathbb{R}^{2nL}$. Note that there are no stability issues in the symmetric case. In this representation, the first nL entries of $\mathbf{e}_i^T f(\mathcal{A}) \mathbf{e}_i$ represent each node-layer pair's broadcaster centrality and the last nL entries of $\mathbf{e}_i^T f(\mathcal{A}) \mathbf{e}_i$ represent each node-layer pair's receiver centrality as it was motivated at the end of Section 3. The only drawback of this approach is that the system size of Equation (5.6) doubles compared to the original problem. However, the nonsymmetric Lanczos method as well as BiCG also require matrix-vector products with the two matrices \mathbf{A} and \mathbf{A}^T in each step, which makes their computational complexities double that of their respective symmetric counterpart. Hence our third approach yields twice as much information as standard methods at the same computational cost.

All three approaches can also be extended to the case $\mathbf{u}^T f(\mathbf{A}) \mathbf{v}$ with $\mathbf{u} \neq \mathbf{v}$. Suitable rules using the nonsymmetric block Lanczos method are discussed in [24]. For the symmetric Lanczos method applied to Equation (5.6) the polarization identity from Equation (5.4) can be used as described in Section 5.2.1. Using Arnoldi's method with a shifted right vector we only have to exchange the left vector in the second step in which we compute $\mathbf{u}^T \mathbf{y}$. In the case of the communicability defined in Equation (3.4) we even have $\mathbf{e}_j^T f(\mathbf{A}) \mathbf{e}_i$ available for free as entries in the vector $\mathbf{y} = f(\mathbf{A}) \mathbf{e}_i = f(\mathbf{A})(\mathbf{e}_i + \mathbf{1}) - f(\mathbf{A}) \mathbf{1}$ computed in the first step for all $j = 1, \dots, nL$.

6. Numerical experiments

We test our approach to generalize matrix function-based centrality measures to layer-coupled multiplex networks by applying it to the following four real world complex multilayer networks:

- Scotland Yard² (undirected, weighted and unweighted versions, $n = 199$, $L = 4$, $nL = 796$, and 468 intra-layer edges)
- Email-EU Department 3³ [46] (directed, weighted, $n = 89$, $L = 18$, $nL = 1602$, and 5005 intra-layer edges)
- European airlines⁴ [17] (undirected, unweighted, $n = 417$, $L = 37$, $nL = 15429$, and 3588 intra-layer edges)

²Multilayer network based on a board game. The network consists of $n = 199$ nodes representing stations in London and $L = 4$ layers representing means of transportation (boat, underground, bus and taxi). Both the weighted and the unweighted adjacency matrix were created by the authors. The weight of each intra-layer edge in the weighted case is determined by the minimal number of taxi rides required to travel between the two connected nodes. The data will be available under <https://github.com/KBergermann/Multiplex-matrix-function-centralities>.

³<https://snap.stanford.edu/data/email-Eu-core-temporal.html>

⁴<http://complex.unizar.es/~atnmultiplex/>

- Twitter Obama⁵ [44] (directed, weighted, $n = 2281259$, $L = 3$, $nL = 6843777$, and 4061960 intra-layer edges)

We start with the small undirected Scotland Yard and the small directed Email-EU data set for which we can compare our numerical methods with “exact” results⁶ and conduct error analyses. The medium-sized European airlines data set allows a comparison of matrix function-based centrality measures with existing results of degree and eigenvector centralities. Finally, the Twitter Obama data set yields an insight into the additional challenges arising in large-scale network computations. The Matlab code implementing all presented numerical experiments will be made publicly available at <https://github.com/KBergermann/Multiplex-matrix-function-centralities>. All run-time measurements were performed on a laptop with 16 GB RAM and an Intel Core i5-8265U CPU with $4 \times 1.60\text{--}3.90$ GHz cores as well as Matlab R2020b.

6.1 Small undirected Scotland Yard data set

We start by considering the small weighted Scotland Yard data set, which consists of $n = 199$ nodes and $L = 4$ layers. The relatively small size of the supra-adjacency matrix $\mathbf{A} \in \mathbb{R}^{796 \times 796}$ permits the explicit evaluation of the full matrix functions. We present the results of selected matrix function-based centrality measures including their dependence on the weighting parameter ω , compare the results obtained by the numerical methods introduced in Section 5 with the explicitly computed results, and compare the runtimes of the different numerical methods.

First, we consider subgraph centrality defined in Equation (3.2). Figure 4a shows a typical distribution of the joint node-layer centralities as it can often be observed for the matrix function-based centralities considered in this paper: the centrality values of the top-ranked node-layer pairs are well-separated and decay quickly; the centrality value distribution is heavy-tailed, i.e. most node-layer pair’s centrality value lies just above $JC(i, l) = 1$, which means that matrix function-based centrality measures tend to localize around the value 1. Localization phenomena of eigenvectors and their impact on diverse network science applications have been studied in the literature, see e.g. [40].

Furthermore, we plot the marginal layer and node subgraph centralities defined in Equations (4.1) and (4.2) where the parameter ω , which trades off the importance of intra- and inter-layer weights is varied in the interval $[10^{-2}, 10^2]$, in Figures 4b and 4c. Note that this type of plots has been used in [53] to illustrate parameter-dependent marginal eigenvector centralities for multiplex and temporal networks. Note also that λ_{\max} depends on ω and needs to be computed separately for each value of ω in order to be able to use a common parameter β for all ω . In our example, the ranking of the importance of both layers and nodes depends only weakly on the inter-layer coupling strength ω . This behavior is often observed for the centrality measures under consideration: the marginal centralities are relatively clearly separated in the weak coupling regime $\omega \rightarrow 0^+$ where all centrality values are dominated by intra-layer weights; in the strong coupling regime $\omega \rightarrow \infty$ all centrality values are dominated by inter-layer weights and in the case of all-to-all coupling without self-edges this leads to a convergence of marginal layer and node centralities to a common limit value. However, we will later encounter numerical examples where marginal centralities are not as ordered for all ω as they are in Figures 4b and 4c but where they

⁵<https://manliodenedomenico.com/data.php>

⁶We rely on the Matlab function `expm` for the matrix exponential and Matlab’s backslash operator for the matrix resolvent function for all explicitly evaluated matrix functions. The so invoked numerical methods, of course, produce approximation as well as rounding errors but for the purpose of our comparison we rely on the high precision of the well-established methods implemented in Matlab.

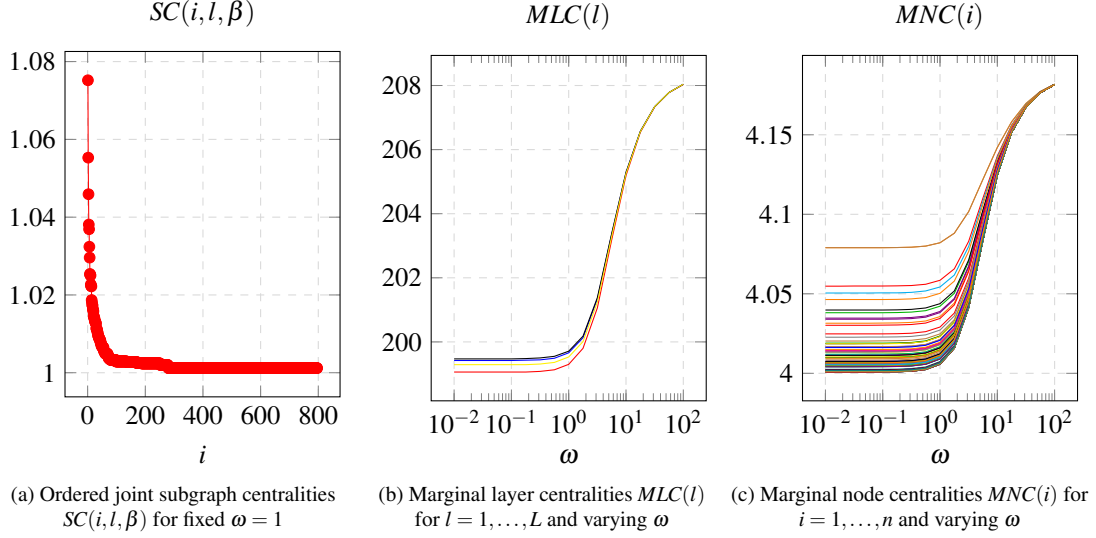


FIG. 4. Joint and marginal subgraph centralities for the weighted undirected Scotland Yard data set with all-to-all inter-layer coupling without self-edges and the parameter $\beta = 0.5/\lambda_{\max}$ for all values of ω .

exhibit a qualitatively different behavior especially in the medium coupling regime.

Next, we compare different centrality measures on the same supra-adjacency matrix and with the same parameters α and β . Table 3 shows that all measures agree on the first four node-layer pairs. The rankings between rank five and ten are similar but there are some deviations. Furthermore the numerical values of the four measures all range in different intervals. Interestingly, total communicability is the only measure with a node-layer pair from another layer but layer 2 in the top 10 joint centralities. The reason that layer two dominates all rankings is that the non-zero intra-layer weights in the second (underground) layer are on average larger than those in the other layers (and anyone who played the game before would probably agree that underground stations are the most central locations in the game).

It is not surprising that many of the top ranked pairs of node-layer pairs of the communicability $C(i, l, j, k, \beta)$ consist of two node-layer pairs, which are among the top-ranked node-layer pairs in all four centrality measures in Table 3. However, Figure 5a also reveals two surprising candidates on ranks three and six: the pair $(153, 2)$ & $(163, 2)$ ranks much higher than would be expected given the individual rankings of the node-layer pairs; even more surprisingly the pair $(157, 1)$ & $(194, 1)$ appears to be very strongly connected although no node-layer pair from layer 1 appears in Table 3. These two node-layer pairs are connected by one of the rare and high-weighted boat edges in layer 1.

Furthermore, we consider the maximal absolute error between joint centralities computed by the numerical methods presented in Sections 5.1 and 5.2.1 and the “exact” results using Matlab’s `expm` function and backslash operator. We define the error

$$\max_{\substack{i \in \{1, \dots, n\} \\ l \in \{1, \dots, L\}}} |XC(i, l, \gamma) - XC_{\text{exact}}(i, l, \gamma)|, \quad (6.1)$$

for $XC \in \{TC, SC, KC, SC_{\text{res}}\}$ and $\gamma \in \{\alpha, \beta\}$, which is used to obtain the error plots in Figures 5b and 5c. Figure 5b compares the four different quadrature rules for subgraph centrality. The obtained

Total communicability		Subgraph centrality		Katz centrality		Resolvent-based subgraph centrality	
(i, l)	$TC(i, l, \beta)$	(i, l)	$SC(i, l, \beta)$	(i, l)	$KC(i, l, \alpha)$	(i, l)	$SC_{\text{res}}(i, l, \alpha)$
(89, 2)	2.0792	(89, 2)	1.0752	(89, 2)	2.7298	(89, 2)	1.2000
(67, 2)	1.9660	(67, 2)	1.0553	(67, 2)	2.5829	(67, 2)	1.1493
(13, 2)	1.7792	(13, 2)	1.0459	(13, 2)	2.2863	(13, 2)	1.1211
(111, 2)	1.7770	(111, 2)	1.0381	(111, 2)	2.1997	(111, 2)	1.0975
(153, 2)	1.7047	(153, 2)	1.0369	(79, 2)	2.0114	(153, 2)	1.0879
(79, 2)	1.6816	(163, 2)	1.0324	(153, 2)	2.0094	(163, 2)	1.0775
(46, 2)	1.6192	(79, 2)	1.0296	(140, 2)	1.9040	(79, 2)	1.0710
(67, 3)	1.6060	(128, 2)	1.0254	(128, 2)	1.8909	(140, 2)	1.0635
(128, 2)	1.5845	(46, 2)	1.0252	(46, 2)	1.8648	(128, 2)	1.0630
(140, 2)	1.5688	(140, 2)	1.0250	(163, 2)	1.8196	(46, 2)	1.0564

Table 3. Top 10 joint centralities of four matrix function-based centrality measures for the weighted undirected Scotland Yard data set with all-to-all inter-layer coupling without self-edges and the parameters $\omega = 1$ and $\alpha = \beta = 0.5/\lambda_{\max}$.

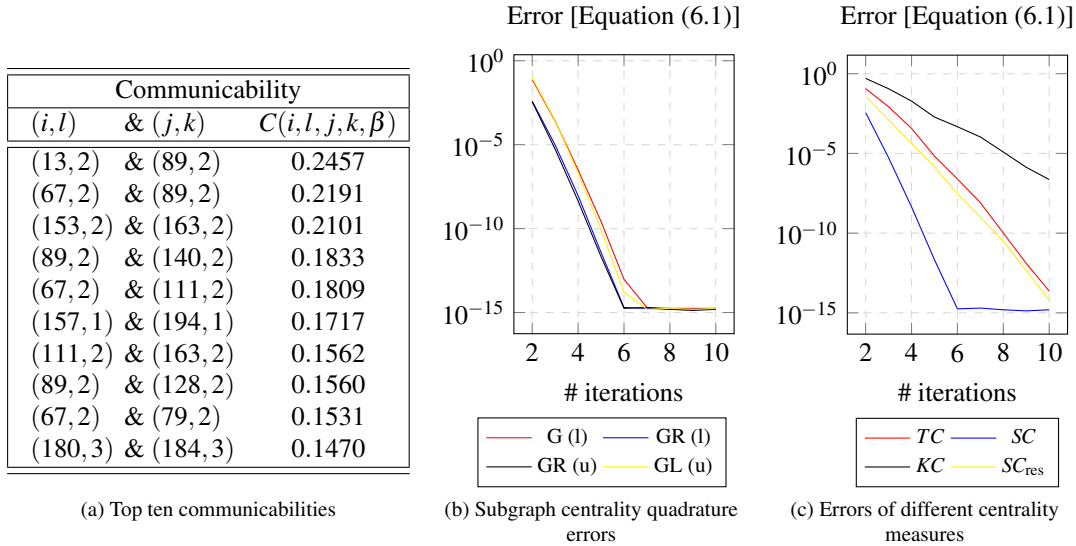


FIG. 5. Communicability results and error plots as by Equation (6.1) for subgraph centrality as well as the four centrality measures from Table 3 for the weighted undirected Scotland Yard data set with all-to-all inter-layer coupling without self-edges and the parameters $\omega = 1$ and $\alpha = \beta = 0.5/\lambda_{\max}$. G stands for Gauss, GR for Gauss–Radau and GL for Gauss–Lobatto quadrature. Furthermore, (l) stands for lower and (u) for upper bound.

errors of the respective bounds are close to machine precision within 6 or 7 Lanczos iterations. The resolvent-based subgraph centrality converges slightly slower: here the symmetric Lanczos method requires around 10 iterations to obtain a similar error. It can often be observed that the Gauss–Radau rules yield somewhat sharper bounds than Gauss and Gauss–Lobatto rules. Furthermore, Figure 5c reveals that also for the quantities $f(\mathbf{A})\mathbf{b}$ the matrix exponential converges faster than the matrix resolvent function. Notably, Gauss–quadrature rules not only yield bounds on the desired quantities but converge much faster than their $f(\mathbf{A})\mathbf{b}$ counterparts. This is in line with theoretical results that after k Krylov iterations the methods presented in Section 5.1 to approximate $f(\mathbf{A})\mathbf{b}$ interpolate polynomials of degree $k - 1$ exactly while the different Gauss quadrature rules from Section 5.2.1 for quantities $\mathbf{u}^T f(\mathbf{A}) \mathbf{u}$ interpolate polynomials of degrees between $2k - 1$ and $2k + 1$ exactly. Note that Figure 5c uses the upper Gauss–Radau rule error. However, the qualitative behavior is the same for the slightly slower converging Gauss or Gauss–Lobatto rules.

As already mentioned in Section 5 we rely on Güttel’s `funm_kryl` toolbox for Matlab [34] for the implementation of the Krylov subspace methods for the evaluation of $f(\mathbf{A})\mathbf{b}$. For the tridiagonalization of \mathbf{A} a few steps of a relatively straight forward implementation of the Lanczos method rapidly yield sufficient results. The quadrature rules can then be computed cheaply as they only require computations involving matrices of the size of the number of Krylov iterations. The runtimes of the quantities $f(\mathbf{A})\mathbf{b}$ of the relatively small Scotland Yard network range up to 0.02 seconds for up to 10 Krylov iterations. For subgraph centrality and the resolvent-based subgraph centrality we need to loop over all $nL = 796$ node-layer pairs. Our Matlab implementation requires around 1 second for up to 10 Lanczos iterations.

6.2 Small directed temporal Email-EU data set

We consider the Department 3 subset of the Email-EU data set [46] as an example for both a temporal network and a small directed network for which all matrix functions can be evaluated explicitly. We demonstrate that the node-layer pairs take different roles as broadcasters and receivers, present results for several matrix function-based centrality measures, conduct empirical error analyses, and discuss runtimes.

The original data set contains the records of 12216 emails, which have been exchanged between $n = 89$ members of a department of a European research institution over a time period of 802 days. As there is a nine month gap between the last 117 and the remaining emails we remove the last 117 emails from the data set. We aggregate the number of emails sent from one individual to another on a monthly basis (with 30 days per month) in order to create a weighted directed temporal multiplex network with the number of emails as weights. The maximal number of emails sent from one individual to another within one month is 47. As the time period remaining after removal of the last 117 records spans over 525 days we obtain $L = 18$ temporal layers. Note that layer 18 only represents a time interval of 15 days. In order to represent the directed temporal relation between the layers we choose forward directed temporal inter-layer coupling, i.e. $\tilde{\mathbf{A}}$ consists of ones on the upper subdiagonal and zeros otherwise.

As discussed in Sections 3 and 5 we obtain broadcaster and receiver centralities for total communicability and Katz centrality considering \mathbf{A} and \mathbf{A}^T , respectively, while subgraph and resolvent-based subgraph centrality applied to the original supra-adjacency matrix in Equation (2.2) do not provide this differentiation. Table 4 lists the top ten joint broadcaster and receiver total communicabilities as well as the top ten resolvent-based subgraph centralities. While some node-layer pairs act as hubs (high broadcaster centrality) and authorities (high receiver centrality) at the same time, other node-layer pairs have a more distinct role in the network. Physical node 71, for instance, ranks as an important hub over the months 6 to 9 apparently without receiving much information in return. Interestingly, not all top

Total communicability				Resolvent-based subgraph centrality	
broadcaster		receiver			
(i, l)	$TC(i, l, \beta)$	(i, l)	$TC(i, l, \beta)$	(i, l)	$SC_{\text{res}}(i, l, \alpha)$
(71, 7)	3.4254	(54, 8)	2.1731	(54, 8)	1.2155
(71, 6)	2.9707	(24, 8)	2.0931	(1, 7)	1.1850
(60, 17)	2.6429	(60, 17)	2.0821	(54, 16)	1.1814
(49, 8)	2.3757	(54, 16)	2.0370	(49, 8)	1.1763
(60, 13)	2.3420	(54, 9)	2.0048	(52, 12)	1.1736
(54, 16)	2.3099	(49, 7)	1.9984	(71, 7)	1.1695
(52, 12)	2.2323	(52, 12)	1.9536	(1, 8)	1.1428
(71, 8)	2.2101	(60, 8)	1.9360	(54, 7)	1.1309
(54, 7)	2.1870	(54, 7)	1.8501	(1, 12)	1.1293
(71, 9)	2.1556	(25, 7)	1.8385	(54, 9)	1.1264

Table 4. Top ten joint broadcaster and receiver total communicabilities and resolvent-based subgraph centralities for the weighted directed Email-EU data set with forward directed temporal inter-layer coupling and parameters $\omega = 1$ and $\alpha = \beta = 0.5/\lambda_{\max}$.

ranked node-layer pairs in resolvent-based subgraph centrality are listed as top hubs or authorities in total communicability.

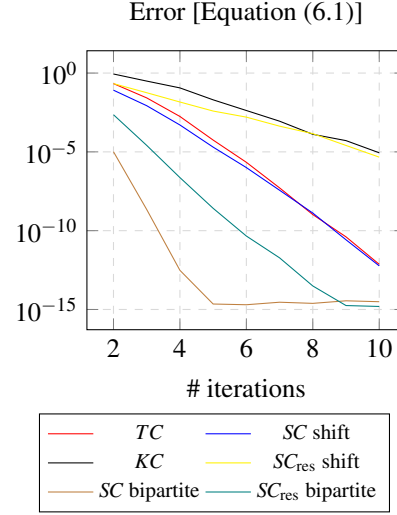
The definition of subgraph and resolvent-based subgraph centrality in the nonsymmetric case can be extended to yield broadcaster and receiver centralities by applying both measure's definition to the symmetric adjacency matrix of the bipartite graph representation of the temporal multiplex network from Equation (5.6). The corresponding results are depicted in Figure 6a. Interestingly, these rankings contain both high ranked hubs and authorities from total communicability as well as high ranked node-layer pairs from the resolvent-based subgraph centrality in Table 4 in the top ten joint broadcaster and receiver centralities.

As already mentioned at the end of Section 4 our temporal network modeling approach in some sense “averages” each physical node's importance in the email communications over the considered period of 525 days when aggregating joint centralities to marginal node centralities. Tracking the development of the intra-layer degree distribution of all physical nodes over time reveals that there is no uniform in- or out-degree distribution for any physical node. Instead, sent and received emails of each individual often strongly vary from month to month. Physical node 9, for instance, hardly communicates via email within the first five months but in the sixth month both the number of sent and received emails suddenly rise to their maxima. This type of temporal development of the network can not be captured by our approach unless we consider different subsets of temporal layers and compare the resulting rankings. Alternatively, dynamical networks [6, 8, 18, 33] could present a valuable tool for this type of problem.

Finally, we investigate the error of our numerical methods defined in Equation (6.1) for the nonsymmetric case compared with the “exact” results computed from the explicitly evaluated matrix functions in dependence of the number of iterations of the respective Krylov subspace method. Recall that the quantities TC and KC are computed by one evaluation of $f(\mathbf{A})\mathbf{b}$, SC shift and SC_{res} shift are computed by Equation (5.5), i.e. two applications of $f(\mathbf{A})\mathbf{b}$, and SC bipartite and SC_{res} bipartite are computed by Gauss quadrature applied to Equation (5.6). Note that whenever broadcaster and receiver centralities are computed we consider the maximal error over all $2nL$ quantities. For most parts, the results qualitatively match those from Figure 5c, i.e. quadrature rules outperform $f(\mathbf{A})\mathbf{b}$ and the exponential tends to

Resolvent-based subgraph centrality			
broadcaster		receiver	
(i, l)	$SC_{\text{res}}(i, l, \alpha)$	(i, l)	$SC_{\text{res}}(i, l, \alpha)$
(71, 7)	1.3325	(66, 7)	1.1104
(71, 6)	1.1428	(1, 7)	1.1029
(71, 9)	1.0702	(9, 7)	1.1012
(71, 8)	1.0622	(54, 8)	1.0587
(49, 8)	1.0595	(66, 6)	1.0556
(70, 2)	1.0513	(20, 2)	1.0512
(54, 7)	1.0482	(9, 6)	1.0467
(52, 12)	1.0463	(49, 7)	1.0394
(71, 12)	1.0460	(54, 9)	1.0335
(57, 1)	1.0446	(1, 8)	1.0299

(a) Top ten broadcaster and receiver resolvent-based subgraph centralities



(b) Errors of different centrality measures

FIG. 6. Left: Top ten joint broadcaster and receiver resolvent-based subgraph centralities for the symmetric bipartite representation of the weighted directed Email-EU data set with forward directed temporal inter-layer coupling and parameters $\omega = 1$ and $\alpha = 0.5/\lambda_{\max}$. Right: Error plots according to Equation (6.1) for the different centrality measures in the nonsymmetric case for the same data set and parameters.

converge faster than the resolvent function. The only notable difference is that SC_{res} bipartite converges faster than TC in these experiments. Furthermore, it is interesting to compare the quantities SC shift and SC_{res} shift (which were not required in the symmetric case) with TC and KC . Recall that SC shift and SC_{res} shift are computed as the difference of a quantity of the form $f(\mathbf{A})\mathbf{b}$ and TC or KC , respectively, where $\mathbf{b} = \mathbf{e}_i + \mathbf{1}$ is very similar to the right vector $\mathbf{1}$ of TC and KC , cf. Equation (5.5). Due to the similarity of these two right vectors the approximation error of Equation (5.1) tends to be similar for both quantities $f(\mathbf{A})(\mathbf{e}_i + \mathbf{1})$ and $f(\mathbf{A})\mathbf{1}$ in Equation (5.5). This leads to the interesting fact that the error of the difference in Equation (5.5) lies below the error of both individual quantities and hence the errors of SC shift and SC_{res} shift in Figure 6b lie slightly below those of TC and KC .

The runtime required for the computation of the quantities TC and KC lies below 0.004 seconds for up to 10 Arnoldi iterations. For SC shift and SC_{res} shift the computation of $nL + 1$ quantities of the form $f(\mathbf{A})\mathbf{b}$ is required which takes up to 1.3 seconds for up to 10 Arnoldi iterations. For SC bipartite and SC_{res} bipartite $2nL$ Lanczos methods with double matrix size and $2nL$ quadrature rules are required. This takes up to 6.5 seconds for up to 10 iterations of the symmetric Lanczos method. For this particular problem the runtime of the nonsymmetric block Lanczos method can not be determined reliably as we encounter serious breakdowns in the computation of centrality measures of node-layer pairs from the first layer. However, using symmetric temporal inter-layer coupling (with ones on both subdiagonals of $\tilde{\mathbf{A}}$ and zeros otherwise) and a block size of 10 leading to $\lceil nL/10 \rceil$ distinct block Lanczos procedures we can compute SC and SC_{res} in up to 2 seconds for up to 10 iterations of the nonsymmetric block Lanczos method.

6.3 Medium-sized undirected European airlines data set

The European airlines data set [17] consists of 450 physical nodes representing European airports and $L = 37$ layers representing European airlines. The network is unweighted and undirected, i.e. the symmetric intra-layer adjacency matrices $\mathbf{A}^{(1)}, \dots, \mathbf{A}^{(37)}$ contain ones where the respective airline offers a flight connection between two airports and zeros otherwise. We discuss runtimes and compare both the top ranked joint centralities and the behavior of marginal node centralities for different weighting parameters ω with existing results from the literature.

We only include the $n = 417$ airports belonging to the largest connected cluster in the sum of the intra-layer adjacency matrices in order to be able to compare our results with eigenvector centralities from [53, Section 5.1]. While this selection is a necessary requirement for the supra-adjacency matrix to satisfy the assumptions of the Perron–Frobenius theorem, which guarantees the uniqueness of the largest eigenvector of the matrix [53, Theorem 3.7], this restriction would not be required for our matrix function-based centrality framework to produce unique results.

While the explicit evaluation of $f(\mathbf{A})$ with $\mathbf{A} = \mathbf{A}^T \in \mathbb{R}^{15429 \times 15429}$ is computationally burdensome and requires approximately 460 seconds using Matlab’s `expm`, it is still feasible to loop over all node-layer pairs and perform quadrature to compute bounds on the diagonal elements $[f(\mathbf{A})]_{ii}$ for $i = 1, \dots, nL$ within a reasonable time frame. For instance, bounds on subgraph centrality of every node-layer pair can be computed in approximately 87 seconds when performing 5 steps of the symmetric Lanczos method per node-layer pair (i.e. 0.006 seconds per node-layer pair) using a relatively straight forward implementation of the Lanczos method. Note that as the matrix-vector products in the tridiagonalization of \mathbf{A} represent the computational bottleneck, quadrature rules computing bounds on resolvent-based subgraph centralities can be added to the computation quite cheaply at only approximately 5% of additional runtime. Furthermore, the node-layer pair-wise computation of quantities of the form $\mathbf{u}^T f(\mathbf{A}) \mathbf{u}$ has great potential for parallelization as an entirely independent Lanczos procedure is employed for each node-layer pair. A very simple parallelization based on the parallel for-loop `parfor` from the Matlab Parallel Computing Toolbox using 4 processes reduces the runtime of 87 seconds to 35 seconds plus a one-time setup of the processes which requires around 20 seconds.

Very few iterations already achieve a notable precision. Table 5 illustrates lower and upper quadrature bounds on the Estrada index defined in Equation (3.3) for the unweighted undirected multiplex European airlines data set with all-to-all inter-layer coupling with self-edges and the parameters $\omega = 1$ and $\beta = 0.5/\lambda_{\max}$. Note that the Estrada index is a sum of $nL = 15429$ individually computed quantities of the form $\mathbf{u}^T f(\mathbf{A}) \mathbf{u}$.

Quantities of the form $f(\mathbf{A})\mathbf{b}$ can be computed in a fraction of seconds. In order to achieve a Lanczos stopping accuracy of 10^{-16} for Katz centrality `funm_kryl` performs 30 iterations with restart length 5 which requires 0.06 seconds. Total communicability only requires 15 iterations with restart length 5 to obtain the stopping accuracy of 10^{-16} which has a runtime of 0.05 seconds. Note that the faster convergence of the matrix exponential is in line with the observations made in Section 6.1.

Similarly to the results of the Scotland Yard data set in Table 3 the same four matrix function-based centrality measures also yield very similar top ten joint centrality rankings for the European airlines data set. Although the numerical values again range in different intervals the top ten of all four measures contain only eleven distinct node-layer pairs. The left column of Table 6 lists the top ten Katz centralities. While resolvent-based subgraph centrality contains the exact same ten node-layer pairs in its top ten ranking in only slightly different order, total communicability and subgraph centrality contain the node-layer pair (Rome, Alitalia) instead of (Bergamo, Ryanair). Table 6 also compares Katz centralities to degree centrality as well as eigenvector centrality as introduced in [53] and implemented

# iterations	1	2	3	4
G (lower)	15 626	15 679.71662	15 679.725281858	15 679.725283509833
GR (lower)	15 671	15 679.72504	15 679.725283471	15 679.725283510321
GR (upper)	15 680	15 679.72568	15 679.725283594	15 679.725283510346
GL (upper)	16 273	15 679.81064	15 679.725296102	15 679.725283511809

Table 5. Bounds on the Estrada index in dependence of the number of Lanczos iterations for the unweighted undirected European airlines data set with all-to-all inter-layer coupling using Gauss (G), Gauss–Radau (GR) and Gauss–Lobatto (GL) quadrature rules with $\omega = 1$ and $\beta = 0.5/\lambda_{\max}$.

Katz centrality		Eigenvector centrality [53]		Degree centrality	
(Stansted, Ryanair)	4.3874	(Frankfurt, Lufthansa)	0.0638	(Stansted, Ryanair)	122
(Munich, Lufthansa)	4.0643	(Munich, Lufthansa)	0.0631	(Atatürk, Turkish)	119
(Frankfurt, Lufthansa)	4.0360	(Amsterdam, KLM)	0.0564	(Munich, Lufthansa)	115
(Atatürk, Turkish)	4.0227	(Düsseldorf, Lufthansa)	0.0530	(Frankfurt, Lufthansa)	114
(Gatwick, easyJet)	3.7676	(Madrid, Iberia)	0.0504	(Gatwick, easyJet)	104
(Dublin, Ryanair)	3.6218	(Vienna, Austrian)	0.0490	(Vienna, Austrian)	101
(Vienna, Austrian)	3.5734	(Paris, Air France)	0.0485	(Amsterdam, KLM)	99
(Amsterdam, KLM)	3.5452	(Madrid, Ryanair)	0.0482	(Dublin, Ryanair)	91
(Bergamo, Ryanair)	3.3037	(Gatwick, easyJet)	0.0472	(Paris, Air France)	87
(Paris, Air France)	3.2280	(Fuimicino, Alitalia)	0.0471	(Fuimicino, Alitalia)	85

Table 6. Top 10 joint centralities of the unweighted undirected European airlines data set with all-to-all inter-layer coupling and parameter $\omega = 1$. The columns contain Katz centrality with the parameter $\alpha = 0.5/\lambda_{\max}$, eigenvector centrality computed with the codes [50], and degree centrality where each degree includes $L = 37$ inter-layer edges of weight 1 from all-to-all coupling.

in the corresponding code release [50]. All degree centralities include $L = 37$ inter-layer edges of weight 1 from all-to-all coupling with the parameter $\omega = 1$. We recall that Section 3 motivated matrix function-based centralities as interpolants between degree and eigenvector centrality. In fact, for the parameter choices $\omega = 1$ and $\beta = 0.5/\lambda_{\max}$ the top ten joint centralities of total communicability and subgraph centrality exactly coincide with the top ten degree ranking. Katz centrality, however, can be seen as a mixture of top-ranked node-layer pairs in eigenvector and degree centrality.

It is interesting to note that the top three Katz marginal node centralities include Madrid and Barcelona airport although both airports do not enter any of the top joint centrality rankings. This situation can only emerge in a constellation where these two airport's importance is well-spread over many different layers, i.e. airlines. Apart from that, marginal and conditional centralities from Equations (4.1) to (4.4) are mainly also dominated by the top ranked node-layer pairs in joint centrality.

The variation of the parameters α and β reveals that the obtained rankings are, over a wide range of values α and β , relatively stable with respect to the parameter ω , which controls the trade-off between intra- and inter-layer weights. This situation leads to the qualitative behavior depicted in Figures 4b and 4c. However, as the parameter $0 < \alpha < 1/\lambda_{\max}$ is increased towards its upper limit the largest eigenvalue λ_{\max} of \mathbf{A} moves closer to the singularity $x = 1/\alpha$ of the resolvent function. Recall that in the symmetric case the matrix functions are applied elementwise to the eigenvalues of \mathbf{A} . This not only increases the numerical values of the corresponding centrality measures but it also leads to a qualitatively

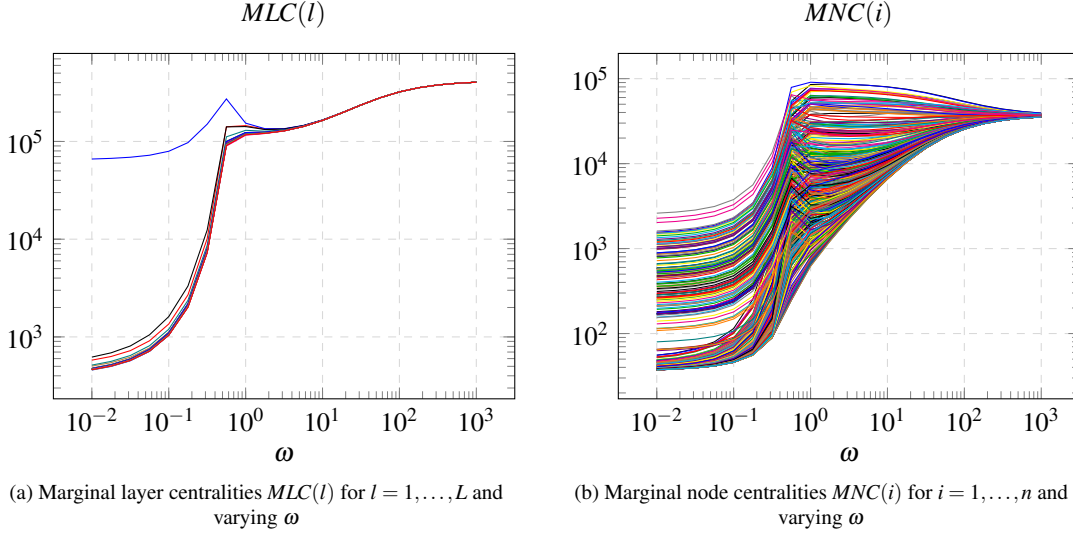


FIG. 7. Marginal layer and node Katz centralities for the unweighted undirected European airlines data set with all-to-all inter-layer coupling and $\alpha = 0.999/\lambda_{\max}$.

different behavior of the marginal centralities. Figures 4b and 4c show that as the parameter ω is varied especially the marginal node centralities undergo strong reordering in the medium coupling regime around $\omega = 1$. This qualitative behavior comes close to that observed in [53, Figure 5] for eigenvector centrality of multiplex networks, which is in line with existing theoretical results. In the single-layer case it has been shown that both Katz and resolvent-based subgraph centrality converge towards eigenvector centrality as $\alpha \rightarrow \frac{1}{\lambda_{\max}}$ [12]. A similar behavior can be observed for $\beta \rightarrow \infty$ in total communicability and subgraph centrality. In the situation of Figures 4b and 4c marginal node centralities appear to be clustered into two groups in the weak coupling regime. The medium coupling regime is characterized by a high degree of reordering before marginal centralities converge to a common value in the strong coupling limit. Interestingly, the strong coupling limit of eigenvector centrality in [53, Figure 5] appears to be characterized by a stabilization of marginal node centralities at well-separated values. In terms of marginal layer centralities both matrix function-based and eigenvector centrality measures have in common that the Ryanair layer is dominant in the weak coupling regime, which is caused by the fact that it contains by far the largest number of intra-layer edges.

6.4 Large directed Twitter Obama data set

Finally, we analyze the relatively large directed Twitter Obama data set [44], which allows to showcase difficulties specific to large-scale network computations.

The data set describes Twitter interactions between $n = 2281\,259$ users which used certain keywords related to Barack Obama's visit in Israel and Palestine in 2013. The three possible types of interactions "retweet", "mention" and "reply" were recorded over the time period between Mar, 19 2013 and Apr, 03 2013. We collect the different types of unilateral interactions between the users in $L = 3$ directed layers and use the number of occurrences between the pairs of individuals as weights. The size of this problem

Broadcaster				Receiver			
(i, l)	$TC(i, l, \beta)$	$SC(i, l, \beta)$	$d(i, l)$	(i, l)	$TC(i, l, \beta)$	$SC(i, l, \beta)$	$d(i, l)$
(111, 1)	1491	16.599	23804	(111, 2)	2254	16.767	31240
(135, 1)	1074	16.560	17508	(164, 2)	2186	17.720	33979
(3997, 1)	975.6	16.352	16142	(111, 3)	1587	16.334	9785
(111, 2)	853.2	16.255	3004	(111, 1)	1380	16.224	3006
(111, 3)	853.0	16.255	3000	(11311, 2)	1262	16.399	15638
(6640, 1)	833.7	16.205	14040	(164, 3)	1231	16.221	3026
(118009, 1)	640.4	16.197	11159	(164, 1)	1230	16.221	3000
(135, 2)	626.6	16.188	3019	(11311, 3)	1143	16.340	11769
(135, 3)	625.9	16.187	3000	(45, 2)	1026	17.320	16674
(3997, 2)	573.2	16.196	3003	(1193, 2)	939.7	17.290	13042

Table 7. Top 10 joint total communicabilities of the weighted directed Twitter Obama data set with all-to-all inter-layer coupling with self-edges and parameters $\omega = 10^3$ and $\beta = 5/\lambda_{\max}$ as well as the corresponding subgraph and degree centralities. The ordering is determined by total communicability values. For degree centrality $d(i, l)$ denotes each node-layer pair's out degree in the case of broadcaster centrality and the in degree in the case of receiver centrality. Note that an inter-layer edge weight of 3000 ($\omega = 10^3$ for $L = 3$ layers) is included in each node-layer pair's in- and out-degree.

poses additional challenges compared to the preceding example data sets. For example, we remark below Equation (2.2) that the explicit formation of the supra-adjacency matrix is computationally not required. As all necessary information is contained in the matrices $\mathbf{A}_{\text{intra}}$ and $\tilde{\mathbf{A}}$, matrix-vector products $\mathbf{A}\mathbf{v}$ with the supra-adjacency matrix \mathbf{A} can be performed by a function taking only $\mathbf{A}_{\text{intra}}$, $\tilde{\mathbf{A}}$, and \mathbf{v} as input. We choose all-to-all inter-layer coupling with self-edges in which case $\mathbf{A}_{\text{intra}}$ and $\tilde{\mathbf{A}}$ consume 114 MB of memory while \mathbf{A} would require 427 MB. Note that this ratio is still relatively low as we only have a 3×3 inter-layer matrix $\tilde{\mathbf{A}}$. As all-to-all coupling contains $\mathcal{O}(L^2)$ non-zeros in $\tilde{\mathbf{A}}$ each of which leads to $n = 2281259$ non-zeros in the supra-adjacency matrix, the explicit storing approach of \mathbf{A} can become a limiting factor on the computable network size.

Despite the high number of node-layer pairs, quantities of the form $f(\mathbf{A})\mathbf{b}$ can still be computed within a few seconds on an average laptop, e.g. total communicability can be computed within approximately 5.5 seconds where 20 Arnoldi iterations with restart length 5 are required in `funm_kryl` to obtain the desired stopping accuracy of 10^{-16} . Choosing relatively small parameters $\beta = 0.5/\lambda_{\max}$ and $\omega = 1$ the top ten broadcaster and receiver total communicabilities exactly coincide with the top ten degree centralities. Increasing both parameters to $\omega = 10^3$ and $\beta = 5/\lambda_{\max}$ has the effect that through the large inter-layer weights the most central physical nodes show up in the top ten rankings with all three instances. Table 7 illustrates that we can thus identify physical node 111 as both the top hub and authority. Furthermore, physical node 135 has the role of the second-most important hub and physical node 164 is identified as the second-most important authority.

Computing subgraph and resolvent-based subgraph centralities for all node-layer pairs is not advisable for this network size. The runtime for one node-layer pair using six iterations of the Lanczos method on the bipartite supra-adjacency matrix from Equation (5.6) for subgraph centrality is approximately 2.8 seconds. Applying this procedure for all $nL = 6843777$ node-layer pairs would require around 222 days. However, subgraph and resolvent-based subgraph centrality can be computed for selected nodes as we demonstrate in Table 7 where we computed $SC(i, l, \beta)$ for the top ten broadcaster and receiver node-layer pairs in total communicability. We observe that both measure's rankings are

very similar for broadcaster centralities but differ significantly for receiver centralities. Interestingly, we observe that total communicability and subgraph centrality do by no means yield as similar top ten joint centrality rankings as they did in earlier examples on smaller data sets. In fact, computing subgraph centrality for the top twenty total communicability hubs and authorities, the top ten subgraph broadcaster centralities already contain two node-layer pairs different from the total communicability top ten and for receiver centrality we already obtain four new node-layer pairs in the top ten. A possible explanation for this behavior is that in the case of smaller networks quantities $f(\mathbf{A})\mathbf{1}$ appear to be dominated by the comparatively large diagonal elements $[f(\mathbf{A})]_{ii}$, whereas for large networks the off-diagonal elements of $f(\mathbf{A})$ contribute much more to the quantity $f(\mathbf{A})\mathbf{1}$. For example, while the ratio between TC and SC in Table 3 is of the order 1.5 to 2 this ratio ranges approximately between 35 and 90 in the case of Table 7. This observation complicates the identification of the top-ranked node-layer pairs in subgraph and resolvent-based subgraph centrality for large-scale networks as it seems unlikely that we capture the most important hubs and authorities in these measures by simple preselection with a “cheap” centrality measure of the form $f(\mathbf{A})\mathbf{b}$.

7. Conclusion and Outlook

We presented an approach to apply matrix function-based centrality measures to layer-coupled multiplex networks using the supra-adjacency matrix as network representation. The interpretation of these centrality measures carries over naturally from the single-layer case. We introduced efficient and scalable numerical methods, which often yield a high precision in only few Krylov subspace iterations. We conducted extensive numerical experiments demonstrating that our approach yields meaningful rankings for nodes, layers, and node-layer pairs for weighted and unweighted as well as directed and undirected multiplex networks. Theoretical results on the convergence speed of numerical methods as well as on the interpolation property of matrix function-based centrality measures between degree and eigenvector centrality were numerically validated. Furthermore, one tuning parameter for the centrality measure and one for the control of the relative importance of inter- and intra-layer weights allow a flexible problem-tailored treatment of data sets from all sorts of applications.

Future work could center around more general multilayer network models in different representations, e.g. tensor representations, as well as the application to various complex problems, which can only be satisfactorily modeled by multilayered structures. Furthermore, randomized linear algebra techniques like stochastic trace estimation may enable the evaluation of measures, which are currently very difficult to access for large-scale networks like, e.g., the Estrada index.

Acknowledgment

M. Stoll acknowledges the funding of the BMBF grant 01-S20053A.

REFERENCES

1. Alon, N., Benjamini, I., Lubetzky, E. & Sodin, S. (2007) Non-backtracking random walks mix faster. *Communications in Contemporary Mathematics*, **9**(4), 585–603.
2. Aprahamian, M., Higham, D. J. & Higham, N. J. (2016) Matching exponential-based and resolvent-based centrality measures. *Journal of Complex Networks*, **4**(2), 157–176.
3. Arnoldi, W. E. (1951) The principle of minimized iterations in the solution of the matrix eigenvalue problem. *Quarterly of applied mathematics*, **9**(1), 17–29.
4. Arrigo, F., Grindrod, P., Higham, D. J. & Noferini, V. (2018a) Non-backtracking walk centrality for directed networks. *Journal of Complex Networks*, **6**(1), 54–78.

5. Arrigo, F., Grindrod, P., Higham, D. J. & Noferini, V. (2018b) On the exponential generating function for non-backtracking walks. *Linear Algebra and its Applications*, **556**, 381–399.
6. Arrigo, F. & Higham, D. J. (2017) Sparse matrix computations for dynamic network centrality. *Applied network science*, **2**(1), 1–19.
7. Barabási, A.-L. & Albert, R. (1999) Emergence of scaling in random networks. *Science*, **286**(5439), 509–512.
8. Benzi, M. & Boito, P. (2020) Matrix functions in network analysis. *GAMM-Mitteilungen*, **43**(3), e202000012.
9. Benzi, M., Estrada, E. & Klymko, C. (2013) Ranking hubs and authorities using matrix functions. *Linear Algebra and its Applications*, **438**(5), 2447–2474.
10. Benzi, M. & Golub, G. H. (1999) Bounds for the entries of matrix functions with applications to preconditioning. *BIT Numerical Mathematics*, **39**(3), 417–438.
11. Benzi, M. & Klymko, C. (2013) Total communicability as a centrality measure. *Journal of Complex Networks*, **1**(2), 124–149.
12. Benzi, M. & Klymko, C. (2015) On the limiting behavior of parameter-dependent network centrality measures. *SIAM Journal on Matrix Analysis and Applications*, **36**(2), 686–706.
13. Bergermann, K., Stoll, M. & Volkmer, T. (2021) Semi-supervised learning for aggregated multilayer graphs using diffuse interface methods and fast matrix vector products. *To appear in: SIAM Journal on Mathematics of Data Science*.
14. Boccaletti, S., Bianconi, G., Criado, R., Del Genio, C. I., Gómez-Gardenes, J., Romance, M., Sendina-Nadal, I., Wang, Z. & Zanin, M. (2014) The structure and dynamics of multilayer networks. *Physics Reports*, **544**(1), 1–122.
15. Bonacich, P. (1987) Power and centrality: A family of measures. *American journal of sociology*, **92**(5), 1170–1182.
16. Brin, S. & Page, L. (1998) The anatomy of a large-scale hypertextual web search engine. *Computer networks and ISDN systems*, **30**(1-7), 107–117.
17. Cardillo, A., Gómez-Gardenes, J., Zanin, M., Romance, M., Papo, D., Del Pozo, F. & Boccaletti, S. (2013) Emergence of network features from multiplexity. *Scientific reports*, **3**(1), 1–6.
18. Chen, I., Benzi, M., Chang, H. H. & Hertzberg, V. S. (2017) Dynamic communicability and epidemic spread: a case study on an empirical dynamic contact network. *Journal of Complex Networks*, **5**(2), 274–302.
19. Estrada, E. (2000) Characterization of 3D molecular structure. *Chemical Physics Letters*, **319**(5-6), 713–718.
20. Estrada, E. (2012) *The structure of complex networks: theory and applications*. Oxford University Press.
21. Estrada, E. & Hatano, N. (2008) Communicability in complex networks. *Physical Review E*, **77**(3), 036111.
22. Estrada, E. & Higham, D. J. (2010) Network properties revealed through matrix functions. *SIAM Review*, **52**(4), 696–714.
23. Estrada, E. & Rodríguez-Velázquez, J. A. (2005) Subgraph centrality in complex networks. *Physical Review E*, **71**(5), 056103.
24. Fenu, C., Martin, D., Reichel, L. & Rodríguez, G. (2013) Block Gauss and anti-Gauss quadrature with application to networks. *SIAM Journal on Matrix Analysis and Applications*, **34**(4), 1655–1684.
25. Freeman, L. C. (1977) A set of measures of centrality based on betweenness. *Sociometry*, **40**(1), 35–41.
26. Freeman, L. C. (1978) Centrality in social networks conceptual clarification. *Social networks*, **1**(3), 215–239.
27. Golub, G. H. & Meurant, G. (1994) Matrices, moments and quadrature. *Pitman Research Notes in Mathematics Series*, **303**, 105–156.
28. Golub, G. H. & Meurant, G. (1997) Matrices, moments and quadrature II; how to compute the norm of the error in iterative methods. *BIT Numerical Mathematics*, **37**(3), 687–705.
29. Golub, G. H. & Meurant, G. (2009) *Matrices, moments and quadrature with applications*. Princeton University Press.
30. Golub, G. H., Stoll, M. & Wathen, A. (2008) Approximation of the scattering amplitude and linear systems. *Electron. Trans. Numer. Anal.*, **31**(2008), 178–203.
31. Golub, G. H. & Van Loan, C. F. (2013) *Matrix computations*, volume 3. JHU press.
32. Golub, G. H. & Welsch, J. H. (1969) Calculation of Gauss quadrature rules. *Mathematics of computation*, **23**(106), 221–230.

33. Grindrod, P., Parsons, M. C., Higham, D. J. & Estrada, E. (2011) Communicability across evolving networks. *Physical Review E*, **83**(4), 046120.
34. Güttel, S. (2008) funm kryl toolbox for Matlab. Available at http://guettel.com/funm_kryl.
35. Higham, N. J. (2008) *Functions of matrices: theory and computation*. SIAM.
36. Katz, L. (1953) A new status index derived from sociometric analysis. *Psychometrika*, **18**(1), 39–43.
37. Kivelä, M., Arenas, A., Barthelemy, M., Gleeson, J. P., Moreno, Y. & Porter, M. A. (2014) Multilayer networks. *Journal of complex networks*, **2**(3), 203–271.
38. Kleinberg, J. M. (1999) Authoritative sources in a hyperlinked environment. *Journal of the ACM (JACM)*, **46**(5), 604–632.
39. Lanczos, C. (1950) *An iteration method for the solution of the eigenvalue problem of linear differential and integral operators*. United States Governm. Press Office Los Angeles, CA.
40. Martin, T., Zhang, X. & Newman, M. E. (2014) Localization and centrality in networks. *Physical review E*, **90**(5), 052808.
41. Milgram, S. (1967) The small world problem. *Psychology today*, **2**(1), 60–67.
42. Moler, C. & Van Loan, C. (2003) Nineteen dubious ways to compute the exponential of a matrix, twenty-five years later. *SIAM Review*, **45**(1), 3–49.
43. Mucha, P. J., Richardson, T., Macon, K., Porter, M. A. & Onnela, J.-P. (2010) Community structure in time-dependent, multiscale, and multiplex networks. *Science*, **328**(5980), 876–878.
44. Omodei, E., De Domenico, M. & Arenas, A. (2015) Characterizing interactions in online social networks during exceptional events. *Frontiers in Physics*, **3**, 59.
45. Page, L., Brin, S., Motwani, R. & Winograd, T. (1999) The PageRank citation ranking: Bringing order to the web. Technical report, Stanford InfoLab.
46. Paranjape, A., Benson, A. R. & Leskovec, J. (2017) Motifs in temporal networks. In *Proceedings of the Tenth ACM International Conference on Web Search and Data Mining*, pages 601–610.
47. Saad, Y. (2003) *Iterative methods for sparse linear systems*. SIAM.
48. Saylor, P. E. & Smolarski, D. C. (2001) Why Gaussian quadrature in the complex plane?. *Numerical Algorithms*, **26**(3), 251–280.
49. Stoll, M. (2020) A literature survey of matrix methods for data science. *GAMM-Mitteilungen*, **43**(3), e202000013.
50. Taylor, D. (2021) Code Release: Supracentrality. Available at <https://github.com/taylordr/Supracentrality>.
51. Taylor, D., Myers, S. A., Clauset, A., Porter, M. A. & Mucha, P. J. (2017) Eigenvector-based centrality measures for temporal networks. *Multiscale Modeling & Simulation*, **15**(1), 537–574.
52. Taylor, D., Porter, M. A. & Mucha, P. J. (2019) Supracentrality analysis of temporal networks with directed interlayer coupling. In *Temporal Network Theory*, pages 325–344. Springer.
53. Taylor, D., Porter, M. A. & Mucha, P. J. (2021) Tunable eigenvector-based centralities for multiplex and temporal networks. *Multiscale Modeling & Simulation*, **19**(1), 113–147.
54. Wang, D., Wang, H. & Zou, X. (2017) Identifying key nodes in multilayer networks based on tensor decomposition. *Chaos: An Interdisciplinary Journal of Nonlinear Science*, **27**(6), 063108.
55. Watts, D. J. & Strogatz, S. H. (1998) Collective dynamics of 'small-world' networks. *Nature*, **393**(6684), 440–442.
56. Wu, M., He, S., Zhang, Y., Chen, J., Sun, Y., Liu, Y.-Y., Zhang, J. & Poor, H. V. (2019) A tensor-based framework for studying eigenvector multicentrality in multilayer networks. *Proceedings of the National Academy of Sciences*, **116**(31), 15407–15413.